

Model Reconstruction Using Counterfactual Explanations: Mitigating the Decision Boundary Shift

Pasan Dissanayake, Sanghamitra Dutta

University of Maryland, College Park

Abstract

Counterfactual explanations find ways of achieving a favorable model outcome with minimum input perturbation. However, counterfactual explanations can also be exploited to steal the model by strategically training a surrogate model to give similar predictions as the original (target) model. In this work, we investigate model extraction by specifically leveraging the fact that *the counterfactual explanations also lie quite close to the decision boundary*. We propose a novel strategy for model extraction that we call Counterfactual Clamping Attack (CCA) which trains a surrogate model using a unique loss function that treats counterfactuals differently than ordinary instances. Our approach also alleviates the related problem of *decision boundary shift* that arises in existing model extraction attacks which treat counterfactuals as ordinary instances. We also derive novel mathematical relationships between the error in model approximation and the number of queries using polytope theory. Experimental results demonstrate that our strategy provides improved fidelity between the target and surrogate model predictions on several real world datasets.

1 Introduction

Counterfactual explanations (Wachter, Mittelstadt, and Russell 2017) are well-known for providing guidance on how to obtain a more favorable outcome from a machine learning model, e.g., increase your income by 10K to qualify for the loan. Given an input instance, a counterfactual explanation (also called a *counterfactual*) finds another instance that belongs to a different output class. Typically, the counterfactual is selected based on certain desirable criteria such as proximity to the original instance, limited feature changes, etc.

While counterfactuals provide several benefits, it has also been shown (Aïvodji, Bolot, and Gambs 2020) that counterfactuals have the potential to leak sensitive information about the underlying model, causing privacy concerns. It can become a serious threat, especially in Machine Learning as a Service (MLaaS) platforms (Gong et al. 2021; Tramèr et al. 2016) that are emerging as a popular alternative to learning models on site, allowing users to query the model for a specified cost (Gong et al. 2020; Juuti et al. 2019). Preserving the privacy of these models is a huge concern for the operators of such services because by strategically querying the model, an adversary may be able to “steal” the model (Wang,

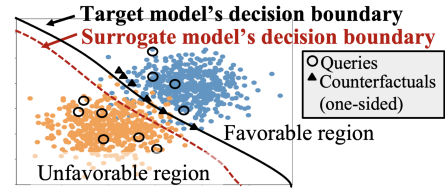


Figure 1: Decision boundary shift in model extraction when counterfactuals are treated as ordinary labeled instances.

Qian, and Miao 2022; Gong et al. 2021; Tramèr et al. 2016; Pal et al. 2020; Juuti et al. 2019). Stealing usually involves training a surrogate model to provide similar predictions as the target model, a practice also referred to as *model extraction*. In this work, our main question is: *How can counterfactuals be leveraged to perform model extraction attacks?*

One existing approach is to treat counterfactuals as ordinary labeled points and use them for training the surrogate model (Aïvodji, Bolot, and Gambs 2020). While this may work for a well-balanced query dataset with queries from the two classes lying roughly equidistant to the decision boundary, it is not the same for unbalanced datasets. The surrogate decision boundary might not always overlap with that of the target model (see Fig. 1), a problem also referred to as a *decision boundary shift*. This is a result of the learning process where the boundary is kept as far as possible from the training examples (margin) to achieve better generalization (Shokri, Strobel, and Zick 2021). This issue is aggravated when the system provides only *one-sided counterfactuals*, i.e., counterfactuals only for queries with unfavorable predictions which is a common use case, e.g., only for rejected applicants in a loan application. This is because the counterfactuals are typically quite close to the decision boundary. *Hence, when treated as ordinary labeled points for training the surrogate model, one-sided counterfactuals make the dataset unbalanced in terms of the distance from the decision boundary.*

In this work, we analyze how model extraction attacks can be refined by specifically leveraging the fact that the counterfactuals are quite close to the decision boundary. We demonstrate strategies that alleviate the decision-boundary-shift issue. We provide novel theoretical guarantees for the attacks,

addressing an important knowledge gap in the existing literature. In contrast to existing attacks Aivodji, Bolot, and Gams (2020) and Wang, Qian, and Miao (2022) which require the system to provide counterfactuals for queries from both sides of the decision boundary, our methods require only one-sided counterfactuals (from one side of the decision boundary). Our contributions can be listed concisely as follows:

- **Fundamental guarantees on model extraction using closest counterfactuals:** We first demonstrate how the closest counterfactuals can provide a linear approximation of the decision boundary around the counterfactuals (Lemma 3.1). Our key contribution lies in analyzing the goodness of this linear approximation *using polytope theory*. We provide a novel theoretical characterization of the relationship between the number of queries and the average agreement of the surrogate model (obtained using linear approximations) with the target model (see Theorem 3.2).
- **An attack based on the proximity of the counterfactuals to the target decision boundary:** Noting the practical challenges associated with generating the closest counterfactual, we focus on an alternative strategy where we exploit only the fact that counterfactuals *lie reasonably close to the decision boundary, but need not be exactly the closest*. We first observe that the Lipschitz continuity of the target and surrogate models would constrict the deviations of their prediction probabilities around matching points (Theorem 3.4). To be precise, if m_1 and m_2 are two Lipschitz continuous classifiers (with Lipschitz constants γ_1 and γ_2 , respectively) and \mathbf{w} is a matching point, i.e., an input instance such that $m_1(\mathbf{w}) = m_2(\mathbf{w})$, then for any \mathbf{x} in the input space, $m_1(\mathbf{x})$ and $m_2(\mathbf{x})$ differ at most by $(\gamma_1 + \gamma_2)\|\mathbf{x} - \mathbf{w}\|_2$. This observation motivates a refined way of utilizing counterfactuals for model extraction. By forcing the surrogate model to match the prediction probabilities of the target model at a sufficiently large number of points along the decision boundary, we can force the decision boundaries of the target and surrogate models to overlap significantly. Furthermore, this can be precisely achieved with counterfactuals because they lie closer to the target decision boundary where the prediction probability of the target model is roughly 0.5. Accordingly, we propose a novel model extraction attack – that we call *Counterfactual Clamping Attack (CCA)* – which introduces a novel loss function for training the surrogate model by clamping its decision boundary to the target decision boundary at the counterfactuals (see Equation 4).
- **Empirical validation:** We conduct experiments on both synthetic datasets, as well as, four real-world datasets, namely, Adult Income (Becker and Kohavi 1996), COMPAS (Angwin et al. 2016), DCCC (Yeh 2016), and HELOC (FICO 2018). Our strategy outperforms the existing strategy in Aivodji, Bolot, and Gams (2020) over all these datasets (Section 4) using one-sided counterfactuals, i.e., counterfactuals only for queries from the unfavorable side of the decision boundary. We also include additional experiments to observe the effects of model architecture, Lipschitzness, and other types of counterfactual generation methods as well as an ablation study to experiment with other loss functions.

Related Works: A plethora of counterfactual-generating mechanisms has been suggested in existing literature (Guidotti 2022; Barocas, Selbst, and Raghavan 2020; Verma et al. 2022; Karimi et al. 2022, 2020; Mothilal, Sharma, and Tan 2020; Dhurandhar et al. 2018; Deutch and Frost 2019; Mishra et al. 2021). Related works that focus on leaking information about the dataset from counterfactual explanations include membership inference attacks (Pawelczyk, Lakkaraju, and Neel 2023) and explanation-linkage attacks (Goethals, Sörensen, and Martens 2023). Shokri, Strobel, and Zick (2021) examines membership inference from other types of explanations, e.g., feature-based. Instead, we focus on model extraction from counterfactual explanations.

Model extraction attacks (without counterfactuals) have been the topic of a wide array of studies (see surveys Gong et al. (2020) and Oliynyk, Mayer, and Rauber (2023)). Various mechanisms such as model inversion (Gong et al. 2021), equation solving (Tramèr et al. 2016), as well as active learning have been considered (Pal et al. 2020). Milli et al. (2019) looks into model reconstruction using other types of explanations, e.g., gradient-based. Yadav, Moshkovitz, and Chaudhuri (2023) explore algorithmic auditing using counterfactual explanations, focusing on linear classifiers and decision trees. Using counterfactual explanations for model extraction has received limited attention, with the notable exception of Aivodji, Bolot, and Gams (2020) and Wang, Qian, and Miao (2022). Aivodji, Bolot, and Gams (2020) suggest using counterfactuals as ordinary labeled examples while training the surrogate model. This suffers from the issue of decision boundary shift, particularly for unbalanced query datasets (one-sided counterfactuals). Wang, Qian, and Miao (2022) introduces a strategy of further querying for the counterfactual of the counterfactual. However, both these methods require the system to provide counterfactuals for queries from both sides of the decision boundary. Nevertheless, a user with a favorable decision may not usually require a counterfactual explanation, and hence a system providing one-sided counterfactuals might be more common, wherein lies our significance. While model extraction attacks (without counterfactuals) have received interest from a theoretical perspective (Tramèr et al. 2016; Papernot et al. 2017; Milli et al. 2019), model extraction attacks involving counterfactual explanations lack such a theoretical understanding. Our work proposes and theoretically analyzes model extraction attacks by explicitly utilizing the fact that the counterfactuals are close to the decision boundary. We provide novel performance guarantees in terms of query complexity for the proposed attacks, leveraging polytope theory, and also address the decision-boundary shift issue.

2 Preliminaries

Notations: We consider binary classification models m that take an input value $\mathbf{x} \in \mathbb{R}^d$ and output a probability between 0 and 1. The final predicted class is denoted by $\lfloor m(\mathbf{x}) \rfloor \in \{0, 1\}$ which is obtained by thresholding the output probability at 0.5 as follows: $\lfloor m(\mathbf{x}) \rfloor = \mathbb{1}[m(\mathbf{x}) \geq 0.5]$ where $\mathbb{1}[\cdot]$ denotes the indicator function. Throughout the paper, we denote the output probability by $m(\mathbf{x})$ and the corresponding thresholded output by $\lfloor m(\mathbf{x}) \rfloor$. Consequently, the deci-

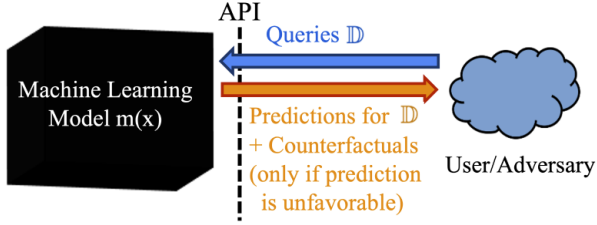


Figure 2: Problem setting

sion boundary of the model m is the $(d-1)$ -dimensional hypersurface (generalization of surface in higher dimensions; see Definition 2.4) in the input space, given by $\partial\mathbb{M} = \{\mathbf{x} : m(\mathbf{x}) = 0.5\}$. We call the region where $\lfloor m(\mathbf{x}) \rfloor = 1$ as the *favorable region* and the region where $\lfloor m(\mathbf{x}) \rfloor = 0$ as the *unfavorable region*. We always state the convexity/concavity of the decision boundary with respect to the favorable region (i.e., the decision boundary is convex if the set $\mathbb{M} = \{\mathbf{x} \in \mathbb{R}^d : \lfloor m(\mathbf{x}) \rfloor = 1\}$ is convex). We assume that upon knowing the range of values for each feature, the d -dimensional input space can be normalized so that the inputs lie within the set $[0, 1]^d$ (the d -dimensional unit hypercube), as is common in literature (Liu et al. 2020; Tramèr et al. 2016; Hamman et al. 2023; Black, Wang, and Fredrikson 2022). We let g_m denote the counterfactual generation mechanism corresponding to the model m .

Definition 2.1 (Counterfactual Generating Mechanism). *Given a cost function $c : [0, 1]^d \times [0, 1]^d \rightarrow \mathbb{R}_0^+$ for measuring the quality of a counterfactual, and a model m , the corresponding counterfactual generating mechanism is the mapping $g_m : [0, 1]^d \rightarrow [0, 1]^d$ specified as*

$$g_m(\mathbf{x}) = \arg \min_{\mathbf{w} \in [0, 1]^d, \lfloor m(\mathbf{w}) \rfloor \neq \lfloor m(\mathbf{x}) \rfloor} c(\mathbf{x}, \mathbf{w}). \quad (1)$$

The cost $c(\mathbf{x}, \mathbf{w})$ is selected based on specific desirable criteria, e.g., $c(\mathbf{x}, \mathbf{w}) = \|\mathbf{x} - \mathbf{w}\|_p$, with $\|\cdot\|_p$ denoting the L_p -norm. Specifically, $p = 2$ leads to the following definition of the *closest counterfactual* (Wachter, Mittelstadt, and Russell 2017; Laugel et al. 2017; Mothilal, Sharma, and Tan 2020).

Definition 2.2 (Closest Counterfactual). *When $c(\mathbf{x}, \mathbf{w}) \equiv \|\mathbf{x} - \mathbf{w}\|_2$, the resulting counterfactual generated using g_m as per Definition 2.1 is called the closest counterfactual.*

Problem Setting: Our problem setting involves a target model m which is pre-trained and assumed to be hosted on a MLaaS platform (see Fig. 2). Users can query it with a set of input instances $\mathbb{D} \subseteq [0, 1]^d$ through an Application Programming Interface (API). The API will provide the users with the set of predictions, i.e., $\{\lfloor m(\mathbf{x}) \rfloor : \mathbf{x} \in \mathbb{D}\}$, and a set of *one-sided* counterfactuals for the instances whose predicted class is 0, i.e., $\{g_m(\mathbf{x}) : \mathbf{x} \in \mathbb{D}, \lfloor m(\mathbf{x}) \rfloor = 0\}$. Note that, by the definition of a counterfactual, $\lfloor m(g_m(\mathbf{x})) \rfloor = 1$ for all \mathbf{x} with $\lfloor m(\mathbf{x}) \rfloor = 0$. An adversary, while appearing to be a normal user, can query with an attack dataset $\mathbb{D}_{\text{attack}} \subseteq [0, 1]^d$ and use the returned labels and counterfactuals to train their own *surrogate model* \tilde{m} . The **goal** of the

adversary is to achieve a certain level of performance with as few queries as possible. In this work, we use *fidelity* as our performance metric for model extraction¹.

Definition 2.3 (Fidelity (Aïvodji, Bolot, and Gamba 2020)). *With respect to a given target model m and a reference dataset $\mathbb{D}_{\text{ref}} \subseteq [0, 1]^d$, the fidelity of a surrogate model \tilde{m} is given by*

$$\text{Fid}_{m, \mathbb{D}_{\text{ref}}}(\tilde{m}) = \frac{1}{|\mathbb{D}_{\text{ref}}|} \sum_{\mathbf{x} \in \mathbb{D}_{\text{ref}}} \mathbb{1}[\lfloor m(\mathbf{x}) \rfloor = \lfloor \tilde{m}(\mathbf{x}) \rfloor].$$

Background on Geometry of Decision Boundaries:

Our theoretical analysis employs arguments based on the geometry of the involved models' decision boundaries. We assume the decision boundaries are hypersurfaces. A hypersurface is a generalization of a surface into higher dimensions, e.g., a line or a curve in a 2-dimensional space, a surface in a 3-dimensional space, etc.

Definition 2.4 (Hypersurface, Lee (2009)). *A hypersurface is a $(d-1)$ -dimensional sub-manifold embedded in \mathbb{R}^d , which can also be denoted by a single implicit equation $\mathcal{S}(\mathbf{x}) = 0$ where $\mathbf{x} \in \mathbb{R}^d$.*

We focus on the properties of hypersurfaces which are "touching" each other, as defined next.

Definition 2.5 (Touching Hypersurfaces). *Let $\mathcal{S}(\mathbf{x}) = 0$ and $\mathcal{T}(\mathbf{x}) = 0$ denote two differentiable hypersurfaces in \mathbb{R}^d . $\mathcal{S}(\mathbf{x}) = 0$ and $\mathcal{T}(\mathbf{x}) = 0$ are said to be touching each other at the point \mathbf{w} if and only if $\mathcal{S}(\mathbf{w}) = \mathcal{T}(\mathbf{w}) = 0$, and there exists a non-empty neighborhood $\mathcal{B}_{\mathbf{w}}$ around \mathbf{w} , such that $\forall \mathbf{x} \in \mathcal{B}_{\mathbf{w}}$ with $\mathcal{S}(\mathbf{x}) = 0$ and $\mathbf{x} \neq \mathbf{w}$, only one of $\mathcal{T}(\mathbf{x}) > 0$ or $\mathcal{T}(\mathbf{x}) < 0$ holds. (i.e., within $\mathcal{B}_{\mathbf{w}}$, $\mathcal{S}(\mathbf{x}) = 0$ and $\mathcal{T}(\mathbf{x}) = 0$ lie on the same side of each other).*

Next, we show that touching hypersurfaces share a common tangent hyperplane at their point of contact. This result is instrumental in exploiting the closest counterfactuals in a model extraction attack (proof in Appendix A.1).

Lemma 2.6. *Let $\mathcal{S}(\mathbf{x}) = 0$ and $\mathcal{T}(\mathbf{x}) = 0$ denote two differentiable hypersurfaces in \mathbb{R}^d , touching each other at point \mathbf{w} . Then, $\mathcal{S}(\mathbf{x}) = 0$ and $\mathcal{T}(\mathbf{x}) = 0$ have a common tangent hyperplane at \mathbf{w} .*

Lipschitz Continuity: Lipschitz continuity, a property that is often encountered in related works (Bartlett, Foster, and Telgarsky 2017; Gouk et al. 2021; Pauli et al. 2021; Hamman et al. 2023; Liu et al. 2020; Marques-Silva et al. 2021), can be exploited in perfecting model extraction attacks.

Definition 2.7 (Lipschitz Continuity). *A model m is said to be Lipschitz continuous with a constant γ if*

$$|m(\mathbf{x}_1) - m(\mathbf{x}_2)| \leq \gamma \|\mathbf{x}_1 - \mathbf{x}_2\|_2 \quad (2)$$

for all $\mathbf{x}_1, \mathbf{x}_2 \in [0, 1]^d$, with $\gamma \in \mathbb{R}_0^+$.

¹Performance can be evaluated using accuracy or fidelity (Jagielski et al. 2020). Accuracy is a measure of how well the surrogate model can predict the true labels over the data manifold of interest. Fidelity measures the agreement between labels predicted by the surrogate and the target models. While attacks based on both measures have been proposed in literature, fidelity-based attacks have been deemed more useful as a first step in designing future attacks (Jagielski et al. 2020; Papernot et al. 2017).

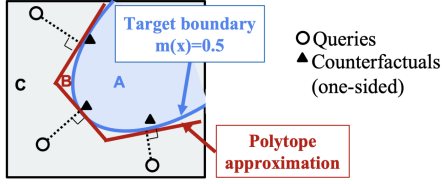


Figure 3: Polytope approximation of a convex decision boundary.

3 Main Results

3.1 Fundamental guarantees on model extraction using closest counterfactuals

We provide a theoretical guarantee on model extraction using the closest counterfactuals in Theorem 3.2. We first start out with demonstrating how the closest counterfactuals provide a linear approximation of *any* decision boundary. Prior work (Yadav, Moshkovitz, and Chaudhuri 2023) shows that for linear models, the line joining a query instance \mathbf{x} and the closest counterfactual \mathbf{w} ($= g_m(\mathbf{x})$) is perpendicular to the linear decision boundary. We generalize this observation to any differentiable decision boundary, not necessarily linear, as follows:

Lemma 3.1. *Let \mathcal{S} denote the decision boundary of a classifier and $\mathbf{x} \in [0, 1]^d$ be any point that is not on \mathcal{S} . Then, the line joining \mathbf{x} and its closest counterfactual \mathbf{w} is perpendicular to \mathcal{S} at \mathbf{w} .*

The proof follows by showing that the d -dimensional ball with radius $\|\mathbf{x} - \mathbf{w}\|_2$ touches (as in Definition 2.5) \mathcal{S} at \mathbf{w} , and invoking Lemma 2.6. For details see Appendix A.1.

As a direct consequence of Lemma 3.1, an adversary may query the system and calculate tangent hyperplanes of the decision boundary drawn at the counterfactual instances. This leads to a linear approximation of the decision boundary (see Fig. 3).

If the decision boundary is convex from the unfavorable side, i.e., the region where $\lfloor m(\mathbf{x}) \rfloor = 0$, such an approximation will provide a set of supporting hyperplanes. *The intersection of these supporting hyperplanes will provide a circumscribing polytope approximation of the decision boundary.* We show that the fidelity of such an approximation, evaluated over uniformly distributed input instances, tends to 1 when the number of counterfactuals is large.

Theorem 3.2. *Let m be the target binary classifier whose decision boundary is convex (i.e., the set $\{\mathbf{x} \in [0, 1]^d : \lfloor m(\mathbf{x}) \rfloor = 1\}$ is convex) and has a continuous second derivative. Denote by \tilde{M}_n , the polytope approximation of m constructed with n supporting hyperplanes obtained through i.i.d. queries. Assume that the fidelity is evaluated with respect to \mathbb{D}_{ref} which is uniformly distributed over $[0, 1]^d$. Then, when $n \rightarrow \infty$ the expected fidelity of \tilde{M}_n with respect to m is given by*

$$\mathbb{E} \left[\text{Fid}_{m, \mathbb{D}_{ref}}(\tilde{M}_n) \right] = 1 - \epsilon \quad (3)$$

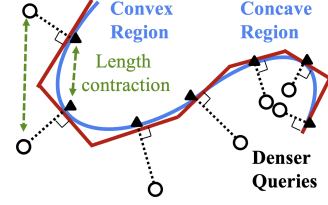


Figure 4: Approximating concave regions need denser queries than convex regions.

where $\epsilon \sim \mathcal{O} \left(n^{-\frac{2}{d-1}} \right)$ and the expectation is over both \tilde{M}_n and \mathbb{D}_{ref} .

The proof utilizes a result from polytope theory (Böröczky Jr and Reitzner 2004) which provides a complexity bound on volume-approximating smooth convex sets by random polytopes. The proof involves observing that the volume of the overlapping decision regions of m and \tilde{M}_n (for example, regions A and C in Fig. 3) translates to the expected fidelity when evaluated under a uniformly distributed \mathbb{D}_{ref} . Appendix A.2 provides the detailed steps.

Remark 3.3 (Relaxing the Convexity Assumption). *Even though Theorem 3.2 assumes convexity of the decision boundary for analytical tractability, the attack can also be extended to a concave decision boundary. This is because the closest counterfactual will always lead to a tangent hyperplane irrespective of convexity and now the rejected region can be seen as the intersection of these half-spaces (Lemma 3.1 does not assume convexity). However, it is worth noting that approximating a concave decision boundary is, in general, more difficult than approximating a convex region. To obtain equally-spaced out tangent hyperplanes on the decision boundary, a concave region will require a much denser set of query points (see Fig. 4) due to the inverse effect of length contraction discussed in Aleksandrov (1967, Chapter III Lemma 2). Furthermore, approximating a decision boundary which is neither convex nor concave is much more challenging as the decision regions can no longer be approximated as intersections of half-spaces.*

We note that the aforementioned attack relies on the closest counterfactual which is often challenging to generate. Practical counterfactual generation mechanisms often provide counterfactuals that are reasonably close but may not be exactly the closest. This motivates us to propose a more general strategy – that we call Counterfactual Clamping Attack (CCA) – that only leverages the fact that the counterfactuals lie closer to the decision boundary but need not be the closest. Experiments indicate that the query complexity of CCA is upper-bounded by the fundamental complexity bound in Theorem 3.2 (see Fig. 14 in Appendix B.2).

3.2 An attack based on the proximity of counterfactuals to the target decision boundary

Before introducing our proposed attack CCA, we first discuss our rationale behind devising this attack. Let us con-

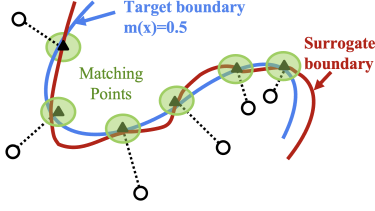


Figure 5: Rationale for Counterfactual Clamping Attack.

sider the difference of the model output probabilities (before thresholding) as a measure of similarity between the target and surrogate models because it would force the decision boundaries to overlap. Our proposed attack CCA is motivated from the following observation: the difference of two models’ output probabilities corresponding to a given input instance \mathbf{x} can be bounded by having another point with matching outputs in the affinity of the instance \mathbf{x} .

Theorem 3.4. *Suppose the target $m(\mathbf{x})$ and the surrogate $\tilde{m}(\mathbf{x})$ are Lipschitz continuous with constants γ_1 and γ_2 , respectively. Assume $m(\mathbf{w}) = \tilde{m}(\mathbf{w})$ for some $\mathbf{w} \in [0, 1]^d$. Then, for any $\mathbf{x} \in [0, 1]^d$, the difference between the outputs of the two models is bounded from above as follows: $|\tilde{m}(\mathbf{x}) - m(\mathbf{x})| \leq (\gamma_1 + \gamma_2) \|\mathbf{x} - \mathbf{w}\|_2$.*

The proof is presented in Appendix A.3. Usually, a smaller Lipschitz constant is indicative of a higher generalizability of a model (Gouk et al. 2021; Pauli et al. 2021).

Remark 3.5 (Local Lipschitz Continuity). *Global Lipschitz continuity is not always necessary. If a well-spread set of points $\mathbb{W} = \{\mathbf{w}_i, i = 1, \dots, N\}$ satisfying $m(\mathbf{w}_i) = \tilde{m}(\mathbf{w}_i)$ for $i = 1, \dots, N$ is available over some region $\mathbb{A} \subseteq [0, 1]^d$, a more relaxed condition of local Lipschitz continuity of m and \tilde{m} in the locality of \mathbf{w}_i ’s is sufficient to ensure the conditions of Theorem 3.4 for all $\mathbf{x} \in \mathbb{A}$.*

Proposed Counterfactual Clamping Attack: Theorem 3.4 provides the motivation for a novel model extraction strategy. Let \mathbf{w} be a counterfactual. Recall that $\partial\mathbb{M}$ denotes the decision boundary of m . As implied by the theorem, for any $\mathbf{x} \in \partial\mathbb{M}$, the deviation of the surrogate model output from the target model output can be bounded above by $(\gamma_1 + \gamma_2) \|\mathbf{x} - \mathbf{w}\|_2$ given that all the counterfactuals satisfy $m(\mathbf{w}) = \tilde{m}(\mathbf{w})$. Knowing that $m(\mathbf{w}) = 0.5$, we may design a loss function which **clamps** $\tilde{m}(\mathbf{w})$ to be 0.5. Consequently, with a sufficient number of well-spaced counterfactuals to cover $\partial\mathbb{M}$, we may achieve arbitrarily small $|\tilde{m}(\mathbf{x}) - m(\mathbf{x})|$ at the decision boundary of m (Fig. 5).

However, we note that simply forcing $\tilde{m}(\mathbf{w})$ to be exactly equal to 0.5 is quite unstable since in practice the target model’s output $m(\mathbf{w})$ is known to be close to 0.5, while being greater but may not be exactly equal. Thus, we propose a unique loss function for training the surrogate neural networks that does not penalize the counterfactuals that are already inside the decision boundary of the surrogate model.

For $0 < k \leq 1$, we define the loss function as

$$L_k(\tilde{m}, y) = \frac{1}{|\mathbb{D}|} \sum_{\mathbf{x} \in \mathbb{D}} \left(\mathbb{1}[y(\mathbf{x}) = 0.5, \tilde{m}(\mathbf{x}) \leq k] \times \left\{ k \log \left(\frac{k}{\tilde{m}(\mathbf{x})} \right) + (1 - k) \log \left(\frac{1 - k}{1 - \tilde{m}(\mathbf{x})} \right) \right\} + \mathbb{1}[y(\mathbf{x}) \neq 0.5] L(\tilde{m}, y) \right). \quad (4)$$

Here, $y(\mathbf{x})$ denotes the label assigned to the input instance \mathbf{x} by the target model, received from the API and $L(\tilde{m}, y)$ is the binary cross-entropy loss. We assume that the counterfactuals are distinguishable from the ordinary instances, and assign them a label of $y(\mathbf{w}) = 0.5$. Here, \mathbb{D} denotes the set of all query instances and the counterfactuals. The first term accounts for the counterfactuals, where they are assigned a non-zero loss if the surrogate model’s prediction is below k . This term ensures $\tilde{m}(\mathbf{w}) \approx k$ for the counterfactuals \mathbf{w} but allows for counterfactuals that lie farther inside the favorable region, which are the result of imperfections in the generating mechanisms. The second term is the ordinary binary cross-entropy loss, which becomes non-zero only for ordinary query instances. Note that substituting $k = 1$ in $L_k(\tilde{m}, y)$ yields the ordinary binary cross entropy loss. Algorithm 1 summarizes the attack proposed above.

Algorithm 1: Proposed Counterfactual Clamping Attack

Require: Attack dataset $\mathbb{D}_{\text{attack}}$, k ($k \in (0, 1]$, usually 0.5), API for querying
Ensure: Trained surrogate model \tilde{m}

- 1: Initialize $\mathbb{A} = \{\}$
- 2: **for** $\mathbf{x} \in \mathbb{D}_{\text{attack}}$ **do**
- 3: Query API with \mathbf{x} to get $y(\mathbf{x})$ $\{y(\mathbf{x}) \in \{0, 1\}\}$
- 4: $\mathbb{A} \leftarrow \mathbb{A} \cup \{(\mathbf{x}, y(\mathbf{x}))\}$
- 5: **if** $y(\mathbf{x}) = 0$ **then**
- 6: Query API for counterfactual \mathbf{w} of \mathbf{x}
- 7: $\mathbb{A} \leftarrow \mathbb{A} \cup \{(\mathbf{w}, 0.5)\}$ {Assign \mathbf{w} a label of 0.5}
- 8: **end if**
- 9: **end for**
- 10: Train \tilde{m} on \mathbb{A} with $L_k(\tilde{m}, y)$ as the loss
- 11: **return** \tilde{m}

Remark 3.6 (Extensions to Other Contours). *This strategy can be extended to approximate any given contour $\partial\mathbb{M}_k = \{\mathbf{x} \in [0, 1]^d : m(\mathbf{x}) = k\}$. It can be helpful in cases where the counterfactual generating algorithm provides counterfactuals that lie on $\partial\mathbb{M}_k$ for some $k > 0.5$, e.g., due to constraints imposed by robustness (Upadhyay, Joshi, and Lakkaraju 2021; Hamman et al. 2023; Black, Wang, and Fredrikson 2022), given that the attacker knows the value of k . When available, the probability predictions received through the API (Tramèr et al. 2016) can be used to fine-tune k .*

It is noteworthy that this approach is different from the broad area of soft-label learning (Nguyen, Valizadegan, and

Hauskrecht 2011; Nguyen et al. 2011) in two major aspects: (i) the labels in our problem do not smoothly span the interval $[0,1]$ – instead they are either 0, 1 or 0.5; (ii) labels of counterfactuals do not indicate a class probability; even though a label of 0.5 is assigned, there can be counterfactuals that are well within the surrogate decision boundary which should not be penalized. Nonetheless, we also perform ablation studies where we compare the performance of our proposed loss function with another potential loss which simply forces $\tilde{m}(w)$ to be exactly 0.5, inspired from soft-label learning (see Appendix B.2 for results).

CCA overcomes two challenges beset in existing works; (i) the problem of decision boundary shift (particularly with one-sided counterfactuals) present in the method suggested by Aivodji, Bolot, and Gams (2020) and (ii) the need for counterfactuals from both sides of the decision boundary in the methods of Aivodji, Bolot, and Gams (2020) and Wang, Qian, and Miao (2022).

4 Experiments

We carry out a number of experiments to study the performance of our proposed strategy CCA. We include some results here and provide further details in Appendix B.

All the classifiers are neural networks unless specified otherwise and their decision boundaries are **not necessarily convex**. We compare the performance of our proposed attack CCA with the existing attack presented in (Aivodji, Bolot, and Gams 2020) that we refer to as “Baseline” for the case of one-sided counterfactuals. As the initial counterfactual generating method, we use an implementation of the Minimum Cost Counterfactuals (MCCF) by Wachter, Mittelstadt, and Russell (2017).

Performance metrics: Fidelity is used for evaluating the agreement between the target and surrogate models. It is evaluated over both uniformly generated instances (denoted by \mathbb{D}_{uni}) and test data instances from the data manifold (denoted by \mathbb{D}_{test}) as the reference dataset \mathbb{D}_{ref} .

Results: A summary of the main experiments is provided below. Additional experiments are detailed in Appendix B.

(i) Visualizing the attack using synthetic data: First, the effect of the proposed loss function in mitigating the decision boundary shift is observed over a 2-D synthetic dataset. Fig. 6 presents the results. In the figure, it is clearly visible that the Baseline model is affected by a decision boundary shift. In contrast, the CCA model’s decision boundary closely approximates the target decision boundary. See Appendix B.2 for more details.

(ii) Comparing performance over four real-world dataset: We use four publicly available real-world datasets namely, Adult Income, COMPAS, DCCC, and HELOC (see Appendix B.1) for our experiments. Table 1 provides some of the results over four real-world datasets. We refer to Appendix B.2 (specifically Fig. 11) for additional results. In all cases, we observe that CCA has either better or similar fidelity as compared to Baseline.

(iii) Studying effects of Lipschitz constants: We study the connection between the target model’s Lipschitz constant and the attack performance. Target model’s Lipschitz

constant is controlled by changing the L_2 -regularization coefficient, while keeping the surrogate models fixed. Results are presented in Fig. 7. Target models with a smaller Lipschitz constant are easier to extract. More details are provided in Appendix B.2.

(iv) Studying different model architectures: We also consider different surrogate model architectures spanning models that are more complex than the target model to much simpler ones. Results show that when sufficiently close to the target model in complexity, the surrogate architecture plays a little role on the performance. Otherwise, the performance degrades. See Fig. 15 and Appendix B.2 for details. Furthermore, two situations are considered where the target model is not a neural network (Fig. 19 and Appendix B.2). In both scenarios, CCA surpasses the baseline.

(v) Studying other counterfactual generating methods: Effects of counterfactuals being sparse, actionable, and realistic are observed. Sparse counterfactuals are generated by using L_1 -norm as the cost function. Actionable counterfactuals are generated using DiCE (Mothilal, Sharma, and Tan 2020) by defining a set of immutable features. Realistic counterfactuals are generated by retrieving the 1-Nearest-Neighbor for a given query from the dataset. The results are given in Table 5 with additional details in Appendix B.2.

(vi) Studying alternate loss functions: We explore using binary cross-entropy loss function directly with labels 0, 1 and 0.5, in place of the proposed loss. However, experiments indicate that this scheme performs poorly when compared with the CCA loss (see Fig. 20 and Appendix B.2).

(vii) Validating Theorem 3.2: Empirical verification of the theorem is done through synthetic experiments, where the model has a spherical decision boundary since they are known to be more difficult for polytope approximation (Arya, Da Fonseca, and Mount 2012). Fig. 8 presents a log-log plot comparing the theoretical and empirical query complexities for several dimensionality values d . The empirical approximation error decays faster than $n^{-2/(d-1)}$ as predicted by the theorem (see Appendix B.3).

5 Conclusion

Our work provides novel insights that bridge explainability and privacy. We introduce novel model extraction strategies aided by counterfactuals, along with the analyses of the corresponding query complexities. The two attacks exploit (i) properties of closest counterfactuals; and (ii) the proximity of the counterfactuals to the target model’s decision boundary, respectively. Our work addresses an important knowledge gap in the existing literature by providing theoretical guarantees using random polytope theory. Furthermore, our attacks address the issue of decision boundary shift amidst a system providing one-sided counterfactuals. Experiments demonstrate a significant improvement in fidelity compared to the baseline method proposed in Aivodji, Bolot, and Gams (2020) for the case of one-sided counterfactuals. Results show that the attack performs well across different model types and counterfactual generating methods. Our findings also highlight an interesting connection between Lipschitz constant and vulnerability to model ex-

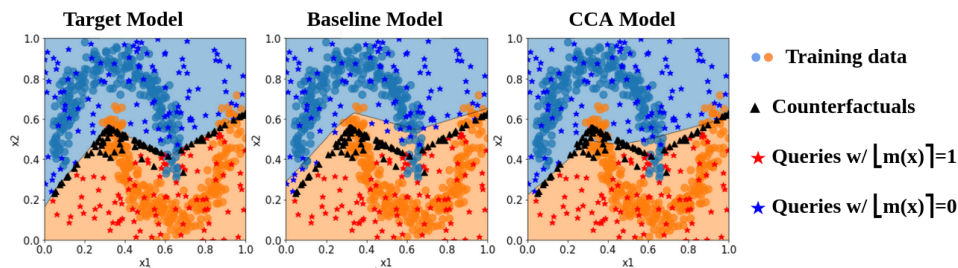


Figure 6: A 2-dimensional demonstration of the proposed attack. Orange and blue shades denote the favorable and unfavorable decision regions of each model. Circles denote the target model’s training data.

Table 1: Fidelity achieved with 400 queries on the real-world datasets. Values presented are the averages \pm standard deviations (as percentages) over an ensemble of size 100. Target model has hidden layers with neurons (20,10). Model 0 is similar to the target model in architecture. Model 1 has hidden layers with neurons (20, 10, 5).

Dataset	Architecture known (model 0)				Architecture unknown (model 1)			
	\mathbb{D}_{test}		\mathbb{D}_{uni}		\mathbb{D}_{test}		\mathbb{D}_{uni}	
	Base.	CCA	Base.	CCA	Base.	CCA	Base.	CCA
Adult In.	91 \pm 3.2	94 \pm 3.2	84 \pm 3.2	91 \pm 3.2	91 \pm 4.5	94 \pm 3.2	84 \pm 3.2	90 \pm 3.2
COMPAS	92 \pm 3.2	96 \pm 2.0	94 \pm 1.7	96 \pm 2.0	91 \pm 8.9	96 \pm 3.2	94 \pm 2.0	94 \pm 8.9
DCCC	89 \pm 8.9	99 \pm 0.9	95 \pm 2.2	96 \pm 1.4	90 \pm 7.7	97 \pm 4.5	95 \pm 2.2	95 \pm 11.8
HELOC	91 \pm 4.7	96 \pm 2.2	92 \pm 2.8	94 \pm 2.4	90 \pm 7.4	95 \pm 5.5	91 \pm 3.3	93 \pm 3.2

traction.

Limitations and future work: Utilizing techniques in active learning in conjunction with counterfactuals is another problem of interest. Extending the results of this work for multi-class classification scenarios can also be explored. The relationship between Lipschitz constant and vulnerability to model extraction may have implications for future work on generalization, adversarial robustness, etc.

One limitation of our theoretical results is the assumption of a convex decision boundary. While this assumption may be satisfied in some settings (Amos, Xu, and Kolter 2017), it is not always the case. In addition, the derivations require the counterfactual generating mechanisms to provide the closest counterfactuals. Any relaxation to these assumptions are paths for exploration. We note that the attack proposed in Section 3.2 remains valid as long as the majority of counterfactuals lie closer to the decision boundary; they need not be the closest ones to the corresponding original instances.

6 Broader Impact

We demonstrate that one-sided counterfactuals can be used for perfecting model extraction attacks, exposing a potential vulnerability in MLaaS platforms. Given the importance of counterfactuals in explaining model predictions, we hope our work will inspire countermeasures and defense strategies, paving the way toward secure and trustworthy machine learning systems.

References

Aïvodji, U.; Bolot, A.; and Gambis, S. 2020. Model extraction from counterfactual explanations. *arXiv preprint arXiv:2009.01884*.

Aleksandrov, A. D. 1967. *A. D. Alexandrov: Selected Works Part II: Intrinsic Geometry of Convex Surfaces*. American Mathematical Society.

Amos, B.; Xu, L.; and Kolter, J. Z. 2017. Input Convex Neural Networks. In *Proceedings of the 34th International Conference on Machine Learning*, 146–155. PMLR. ISSN: 2640-3498.

Angwin, J.; Larson, J.; Mattu, S.; and Kirchner, L. 2016. *Machine Bias*. ProPublica.

Arya, S.; Da Fonseca, G. D.; and Mount, D. M. 2012. Polytope Approximation and the Mahler Volume. In *Proceedings of the Twenty-Third Annual ACM-SIAM Symposium on Discrete Algorithms*, 29–42. Society for Industrial and Applied Mathematics.

Barocas, S.; Selbst, A. D.; and Raghavan, M. 2020. The hidden assumptions behind counterfactual explanations and principal reasons. In *Proceedings of the 2020 Conference on Fairness, Accountability, and Transparency*, 80–89.

Bartlett, P. L.; Foster, D. J.; and Telgarsky, M. J. 2017. Spectrally-normalized margin bounds for neural networks. In *Advances in Neural Information Processing Systems*, volume 30.

Becker, B.; and Kohavi, R. 1996. Adult. UCI Machine Learning Repository. DOI: <https://doi.org/10.24432/C5XW20>.

Black, E.; Wang, Z.; and Fredrikson, M. 2022. Consistent Counterfactuals for Deep Models. In *International Conference on Learning Representations*.

Böröczky Jr, K.; and Reitzner, M. 2004. Approximation of smooth convex bodies by random circumscribed polytopes. *The Annals of Applied Probability*, 14(1): 239–273.

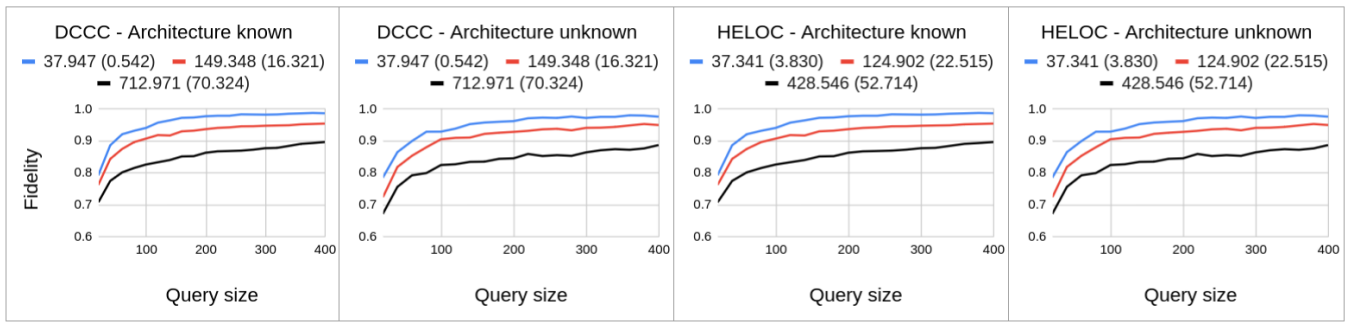


Figure 7: Dependence of fidelity on the target model’s Lipschitz constant. The approximations of the Lipschitz constants are shown in the legend with standard deviations within brackets. Lipschitz constants are approximated as the product of the spectral norm of weight matrices in each model. With a higher Lipschitz constant, the fidelity achieved by a given number of queries tend to degrade.

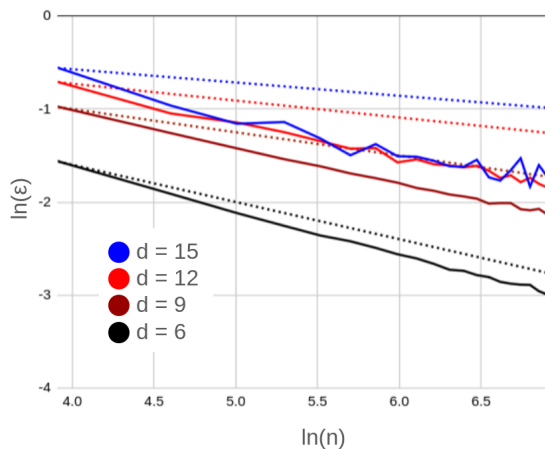


Figure 8: Verifying Theorem 3.2: Dotted and solid lines indicate the theoretical and empirical rates of convergence.

Deutch, D.; and Frost, N. 2019. Constraints-based explanations of classifications. In *IEEE 35th International Conference on Data Engineering*, 530–541.

Dhurandhar, A.; Chen, P.-Y.; Luss, R.; Tu, C.-C.; Ting, P.; Shanmugam, K.; and Das, P. 2018. Explanations based on the missing: Towards contrastive explanations with pertinent negatives. In *Advances in Neural Information Processing Systems*, volume 31.

FICO. 2018. Explainable Machine Learning Challenge.

Goethals, S.; Sörensen, K.; and Martens, D. 2023. The privacy issue of counterfactual explanations: Explanation linkage attacks. *ACM Transactions on Intelligent Systems and Technology*, 14(5): 1–24.

Gong, X.; Chen, Y.; Yang, W.; Mei, G.; and Wang, Q. 2021. InverseNet: Augmenting Model Extraction Attacks with Training Data Inversion. In *Proceedings of the Thirtieth International Joint Conference on Artificial Intelligence*, 2439–2447.

Gong, X.; Wang, Q.; Chen, Y.; Yang, W.; and Jiang, X. 2020. Model extraction attacks and defenses on cloud-based ma-

chine learning models. *IEEE Communications Magazine*, 58(12): 83–89.

Gouk, H.; Frank, E.; Pfahringer, B.; and Cree, M. J. 2021. Regularisation of neural networks by enforcing lipschitz continuity. *Machine Learning*, 110: 393–416.

Guidotti, R. 2022. Counterfactual explanations and how to find them: Literature review and benchmarking. *Data Mining and Knowledge Discovery*, 1–55.

Hamman, F.; Noorani, E.; Mishra, S.; Magazzeni, D.; and Dutta, S. 2023. Robust Counterfactual Explanations for Neural Networks With Probabilistic Guarantees. In *40th International Conference on Machine Learning*.

Jagielski, M.; Carlini, N.; Berthelot, D.; Kurakin, A.; and Papernot, N. 2020. High accuracy and high fidelity extraction of neural networks. In *Proceedings of the 29th USENIX Conference on Security Symposium*, 1345–1362.

Juuti, M.; Szyller, S.; Marchal, S.; and Asokan, N. 2019. PRADA: Protecting against DNN model stealing attacks. In *2019 IEEE European Symposium on Security and Privacy*, 512–527.

Karimi, A.-H.; Barthe, G.; Balle, B.; and Valera, I. 2020. Model-agnostic counterfactual explanations for consequential decisions. In *International Conference on Artificial Intelligence and Statistics*, 895–905.

Karimi, A.-H.; Barthe, G.; Schölkopf, B.; and Valera, I. 2022. A survey of algorithmic recourse: Contrastive explanations and consequential recommendations. *ACM Computing Surveys*, 55(5): 1–29.

Laugel, T.; Lesot, M.-J.; Marsala, C.; Renard, X.; and Delyniecki, M. 2017. Inverse classification for comparison-based interpretability in machine learning. *arXiv preprint arXiv:1712.08443*.

Lee, J. M. 2009. *Manifolds and Differential Geometry*. Graduate Studies in Mathematics. American Mathematical Society.

Liu, X.; Han, X.; Zhang, N.; and Liu, Q. 2020. Certified Monotonic Neural Networks. In *Advances in Neural Information Processing Systems*, volume 33, 15427–15438.

- Marques-Silva, J.; Gerspacher, T.; Cooper, M. C.; Ignatiev, A.; and Narodytska, N. 2021. Explanations for Monotonic Classifiers. In *38th International Conference on Machine Learning*.
- Milli, S.; Schmidt, L.; Dragan, A. D.; and Hardt, M. 2019. Model reconstruction from model explanations. In *Proceedings of the Conference on Fairness, Accountability, and Transparency*, 1–9.
- Mishra, S.; Dutta, S.; Long, J.; and Magazzeni, D. 2021. A Survey on the Robustness of Feature Importance and Counterfactual Explanations. *arXiv e-prints*, arXiv:2111.00358.
- Mothilal, R. K.; Sharma, A.; and Tan, C. 2020. Explaining Machine Learning Classifiers through Diverse Counterfactual Explanations. In *Proceedings of the 2020 Conference on Fairness, Accountability, and Transparency*.
- Nguyen, Q.; Valizadegan, H.; and Hauskrecht, M. 2011. Learning classification with auxiliary probabilistic information. *IEEE International Conference on Data Mining*, 2011: 477–486.
- Nguyen, Q.; Valizadegan, H.; Seybert, A.; and Hauskrecht, M. 2011. Sample-efficient learning with auxiliary class-label information. *AMIA Annual Symposium Proceedings*, 2011: 1004–1012.
- Oliynyk, D.; Mayer, R.; and Rauber, A. 2023. I Know What You Trained Last Summer: A Survey on Stealing Machine Learning Models and Defences. *ACM Computing Surveys*, 55(14s).
- Pal, S.; Gupta, Y.; Shukla, A.; Kanade, A.; Shevade, S.; and Ganapathy, V. 2020. Activethief: Model extraction using active learning and unannotated public data. In *Proceedings of the AAAI Conference on Artificial Intelligence*, volume 34, 865–872.
- Papernot, N.; McDaniel, P.; Goodfellow, I.; Jha, S.; Celik, Z. B.; and Swami, A. 2017. Practical black-box attacks against machine learning. In *Proceedings of the 2017 ACM on Asia Conference on Computer and Communications Security*, 506–519.
- Pauli, P.; Koch, A.; Berberich, J.; Kohler, P.; and Allgöwer, F. 2021. Training robust neural networks using Lipschitz bounds. *IEEE Control Systems Letters*, 6: 121–126.
- Pawelczyk, M.; Lakkaraju, H.; and Neel, S. 2023. On the Privacy Risks of Algorithmic Recourse. In *Proceedings of the 26th International Conference on Artificial Intelligence and Statistics*, volume 206, 9680–9696.
- Shokri, R.; Strobel, M.; and Zick, Y. 2021. On the privacy risks of model explanations. In *Proceedings of the 2021 AAAI/ACM Conference on AI, Ethics, and Society*, 231–241.
- Tramèr, F.; Zhang, F.; Juels, A.; Reiter, M. K.; and Ristenpart, T. 2016. Stealing machine learning models via prediction APIs. In *25th USENIX Security Symposium*, 601–618.
- Upadhyay, S.; Joshi, S.; and Lakkaraju, H. 2021. Towards robust and reliable algorithmic recourse. *Advances in Neural Information Processing Systems*, 34: 16926–16937.
- Verma, S.; Boonsanong, V.; Hoang, M.; Hines, K. E.; Dickerson, J. P.; and Shah, C. 2022. Counterfactual Explanations and Algorithmic Recourses for Machine Learning: A Review. *arXiv preprint arXiv:2010.10596*.
- Wachter, S.; Mittelstadt, B.; and Russell, C. 2017. Counterfactual Explanations without Opening the Black Box: Automated Decisions and the GDPR. *Harvard Journal of Law and Technology*, 31: 841.
- Wang, Y.; Qian, H.; and Miao, C. 2022. DualCF: Efficient Model Extraction Attack from Counterfactual Explanations. In *2022 ACM Conference on Fairness, Accountability, and Transparency*, 1318–1329.
- Yadav, C.; Moshkovitz, M.; and Chaudhuri, K. 2023. XAudit : A Theoretical Look at Auditing with Explanations. *arXiv:2206.04740*.
- Yeh, I.-C. 2016. Default of Credit Card Clients. UCI Machine Learning Repository. DOI: <https://doi.org/10.24432/C55S3H>.

A Proofs

A.1 Proof of Lemma 2.6 and Lemma 3.1

Lemma 2.6. *Let $S(\mathbf{x}) = 0$ and $T(\mathbf{x}) = 0$ denote two differentiable hypersurfaces in \mathbb{R}^d , touching each other at point \mathbf{w} . Then, $S(\mathbf{x}) = 0$ and $T(\mathbf{x}) = 0$ have a common tangent hyperplane at \mathbf{w} .*

Proof. From Definition 2.5, there exists a non-empty neighborhood $\mathcal{B}_{\mathbf{w}}$ around \mathbf{w} , such that $\forall \mathbf{x} \in \mathcal{B}_{\mathbf{w}}$ with $S(\mathbf{x}) = 0$ and $\mathbf{x} \neq \mathbf{w}$, only one of $T(\mathbf{x}) > 0$ or $T(\mathbf{x}) < 0$ holds. Let $\mathbf{x} = (x_1, x_2, \dots, x_d)$ and $\mathbf{x}_{[p]}$ denote \mathbf{x} without x_p for $1 \leq p \leq d$. Then, within the neighborhood $\mathcal{B}_{\mathbf{w}}$, we may re-parameterize $S(\mathbf{x}) = 0$ as $x_p = S(\mathbf{x}_{[p]})$. Note that a similar re-parameterization denoted by $x_p = T(\mathbf{x}_{[p]})$ can be applied to $T(\mathbf{x}) = 0$ as well. Let $\mathcal{A}_{\mathbf{w}} = \{\mathbf{x}_{[p]} : \mathbf{x} \in \mathcal{B}_{\mathbf{w}} \setminus \{\mathbf{w}\}\}$. From Definition 2.5, all $\mathbf{x} \in \mathcal{B}_{\mathbf{w}} \setminus \{\mathbf{w}\}$ satisfy only one of $T(\mathbf{x}) < 0$ or $T(\mathbf{x}) > 0$, and hence without loss of generality the re-parameterization of $T(\mathbf{x}) = 0$ can be such that $S(\mathbf{x}_{[p]}) < T(\mathbf{x}_{[p]})$ holds for all $\mathbf{x}_{[p]} \in \mathcal{A}_{\mathbf{w}}$. Now, define $F(\mathbf{x}_{[p]}) \equiv T(\mathbf{x}_{[p]}) - S(\mathbf{x}_{[p]})$. Observe that $F(\mathbf{x}_{[p]})$ has a minimum at \mathbf{w} and hence, $\nabla_{\mathbf{x}_{[p]}} F(\mathbf{w}_{[p]}) = 0$. Consequently, $\nabla_{\mathbf{x}_{[p]}} T(\mathbf{w}_{[p]}) = \nabla_{\mathbf{x}_{[p]}} S(\mathbf{w}_{[p]})$, which implies that the tangent hyperplanes to both hypersurfaces have the same gradient at \mathbf{w} . Proof concludes by observing that since both tangent hyperplanes go through \mathbf{w} , the two hypersurfaces should share a common tangent hyperplane at \mathbf{w} . \square

Lemma 3.1. *Let S denote the decision boundary of a classifier and $\mathbf{x} \in [0, 1]^d$ be any point that is not on S . Then, the line joining \mathbf{x} and its closest counterfactual \mathbf{w} is perpendicular to S at \mathbf{w} .*

Proof. The proof utilizes the following lemma.

Lemma A.1. *Consider the d -dimensional ball $\mathcal{C}_{\mathbf{x}}$ centered at \mathbf{x} , with \mathbf{w} lying on its boundary (hence $\mathcal{C}_{\mathbf{x}}$ intersects S at \mathbf{w}). Then, S lies completely outside $\mathcal{C}_{\mathbf{x}}$.*

The proof of Lemma A.1 follows from the following contradiction. Assume a part of S lies within $\mathcal{C}_{\mathbf{x}}$. Then, points on the intersection of S and the interior of $\mathcal{C}_{\mathbf{x}}$ are closer to \mathbf{x} than \mathbf{w} . Hence, \mathbf{w} can no longer be the closest point to \mathbf{x} , on S .

From Lemma A.1, $\mathcal{C}_{\mathbf{x}}$ is touching the curve S at \mathbf{w} , and hence, they share the same tangent hyperplane at \mathbf{w} by Lemma 2.6. Now, observing that the line joining \mathbf{w} and \mathbf{x} , being a radius of $\mathcal{C}_{\mathbf{x}}$, is the normal to the ball at \mathbf{w} concludes the proof (see Fig. 9). \square

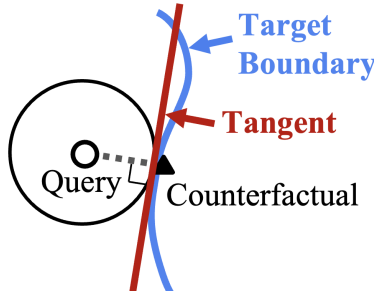


Figure 9: Line joining the query and its closest counterfactual is perpendicular to the decision boundary at the counterfactual. See Lemma 3.1 for details.

We present the following corollary as an additional observation resulting from Lemma A.1.

Corollary A.2. *Following Lemma A.1, it can be seen that all the points in the d -dimensional ball with \mathbf{x} as the center and \mathbf{w} on boundary lies on the same side of S as \mathbf{x} .*

A.2 Proof of Theorem 3.2

Theorem 3.2. *Let m be the target binary classifier whose decision boundary is convex (i.e., the set $\{\mathbf{x} \in [0, 1]^d : \lfloor m(\mathbf{x}) \rfloor = 1\}$ is convex) and has a continuous second derivative. Denote by \tilde{M}_n , the polytope approximation of m constructed with n supporting hyperplanes obtained through i.i.d. queries. Assume that the fidelity is evaluated with respect to \mathbb{D}_{ref} which is uniformly distributed over $[0, 1]^d$. Then, when $n \rightarrow \infty$ the expected fidelity of \tilde{M}_n with respect to m is given by*

$$\mathbb{E} \left[\text{Fid}_{m, \mathbb{D}_{ref}}(\tilde{M}_n) \right] = 1 - \epsilon \quad (3)$$

where $\epsilon \sim \mathcal{O} \left(n^{-\frac{2}{d-1}} \right)$ and the expectation is over both \tilde{M}_n and \mathbb{D}_{ref} .

Proof. We first have a look at Böröczky Jr and Reitzner (2004, Theorem 1 (restated as Theorem A.3 below)) from the polytope theory. Let \mathbb{M} be a compact convex set with a second-order differentiable boundary denoted by $\partial\mathbb{M}$. Let $\mathbf{a}_1, \dots, \mathbf{a}_n$ be n randomly chosen points on $\partial\mathbb{M}$, distributed independently and identically according to a given density $d_{\partial\mathbb{M}}$. Denote by $H_+(\mathbf{a}_i)$ the supporting hyperplane of $\partial\mathbb{M}$ at \mathbf{a}_i . Assume C to be a large enough hypercube which contains \mathbb{M} in its interior.

Now, define

$$\tilde{\mathbb{M}}_n = \bigcap_{i=1}^n H_+(\mathbf{a}_i) \cap C \quad (5)$$

which is the polytope created by the intersection of all the supporting hyperplanes. The theorem characterizes the expected difference of the volumes of \mathbb{M} and $\tilde{\mathbb{M}}_n$.

Theorem A.3 (Random Polytope Approximation, (Böröczky Jr and Reitzner 2004)). *For a convex compact set \mathbb{M} with second-order differentiable $\partial\mathbb{M}$ and non-zero continuous density $d_{\partial\mathbb{M}}$,*

$$\mathbb{E} \left[V(\tilde{\mathbb{M}}_n) - V(\mathbb{M}) \right] = \tau(\partial\mathbb{M}, d) n^{-\frac{2}{d-1}} + o\left(n^{-\frac{2}{d-1}}\right) \quad (6)$$

as $n \rightarrow \infty$, where $V(\cdot)$ denotes the volume (i.e., the Lebesgue measure), and $\tau(\partial\mathbb{M}, d)$ is a constant that depends only on the boundary $\partial\mathbb{M}$ and the dimensionality d of the space.

Let $\mathbf{x}_i, i = 1, \dots, n$ be n i.i.d queries from the $\lfloor m(\mathbf{x}) \rfloor = 0$ region of the target model. Then, their corresponding counterfactuals $g_m(\mathbf{x}_i)$ are also i.i.d. Furthermore, they lie on the decision boundary of m . Hence, we may arrive at the following result.

Corollary A.4. *Let $\mathbb{M} = \{\mathbf{x} \in [0, 1]^d : \lfloor m(\mathbf{x}) \rfloor = 1\}$ and $\tilde{\mathbb{M}}_n = \{\mathbf{x} \in [0, 1]^d : \lfloor \tilde{M}_n(\mathbf{x}) \rfloor = 1\}$. Then, by Theorem A.3,*

$$\mathbb{E} \left[V(\tilde{\mathbb{M}}_n) - V(\mathbb{M}) \right] \sim \mathcal{O}\left(n^{-\frac{2}{d-1}}\right) \quad (7)$$

when $n \rightarrow \infty$. Note that $\mathbb{M} \subseteq \tilde{\mathbb{M}}_n$ and hence, the left-hand side is always non-negative.

From Definition 2.3, we may write

$$\begin{aligned} & \mathbb{E} \left[\text{Fid}_{m, \mathbb{D}_{\text{ref}}}(\tilde{M}_n) \right] \\ &= \mathbb{E} \left[\frac{1}{|\mathbb{D}_{\text{ref}}|} \sum_{\mathbf{x} \in \mathbb{D}_{\text{ref}}} \mathbb{E} \left[\mathbb{1} \left[\lfloor m(\mathbf{x}) \rfloor = \lfloor \tilde{M}_n(\mathbf{x}) \rfloor \right] \mid \mathbb{D}_{\text{ref}} \right] \right] \end{aligned} \quad (8)$$

$$= \frac{1}{|\mathbb{D}_{\text{ref}}|} \mathbb{E} \left[\sum_{\mathbf{x} \in \mathbb{D}_{\text{ref}}} \mathbb{P} \left[\lfloor m(\mathbf{x}) \rfloor = \lfloor \tilde{M}_n(\mathbf{x}) \rfloor \mid \mathbf{x} \right] \right] \quad (\because \text{query size is fixed}) \quad (9)$$

$$= \mathbb{P} \left[\lfloor m(\mathbf{x}) \rfloor = \lfloor \tilde{M}_n(\mathbf{x}) \rfloor \right] \quad (\because \mathbf{x}'\text{s are i.i.d.}) \quad (10)$$

$$= \int_{\mathcal{M}_n} \mathbb{P} \left[\lfloor m(\mathbf{x}) \rfloor = \lfloor \tilde{M}_n(\mathbf{x}) \rfloor \mid \tilde{M}_n(\mathbf{x}) = \tilde{m}_n(\mathbf{x}) \right] \mathbb{P} \left[\tilde{M}_n(\mathbf{x}) = \tilde{m}_n(\mathbf{x}) \right] d\tilde{m}_n \quad (11)$$

where \mathcal{M}_n is the set of all possible \tilde{m}_n 's.

Now, by noting that

$$\mathbb{P} \left[\lfloor m(\mathbf{x}) \rfloor = \lfloor \tilde{M}_n(\mathbf{x}) \rfloor \mid \tilde{M}_n(\mathbf{x}) = \tilde{m}_n(\mathbf{x}) \right] = 1 - \mathbb{P} \left[\lfloor m(\mathbf{x}) \rfloor \neq \lfloor \tilde{M}_n(\mathbf{x}) \rfloor \mid \tilde{M}_n(\mathbf{x}) = \tilde{m}_n(\mathbf{x}) \right], \quad (12)$$

we may obtain

$$\begin{aligned} \mathbb{E} \left[\text{Fid}_{m, \mathbb{D}_{\text{ref}}}(\tilde{M}_n) \right] &= 1 - \int_{\mathcal{M}_n} \mathbb{P} \left[\lfloor m(\mathbf{x}) \rfloor \neq \lfloor \tilde{M}_n(\mathbf{x}) \rfloor \mid \tilde{M}_n(\mathbf{x}) = \tilde{m}_n(\mathbf{x}) \right] \\ &\quad \times \mathbb{P} \left[\tilde{M}_n(\mathbf{x}) = \tilde{m}_n(\mathbf{x}) \right] d\tilde{m}_n \end{aligned} \quad (13)$$

$$\begin{aligned} &= 1 - \int_{\mathcal{M}_n} \underbrace{\frac{V(\tilde{\mathbb{M}}_n) - V(\mathbb{M})}{\text{Total volume}}}_{=1 \text{ for unit hypercube}} \mathbb{P} \left[\tilde{M}_n(\mathbf{x}) = \tilde{m}_n(\mathbf{x}) \right] d\tilde{m}_n \\ &\quad (\because \mathbf{x}'\text{s are uniformly distributed}) \end{aligned} \quad (14)$$

$$= 1 - \mathbb{E} \left[V(\tilde{\mathbb{M}}_n) - V(\mathbb{M}) \right]. \quad (15)$$

The above result, in conjunction with Corollary A.4, concludes the proof. \square

A.3 Proof of Theorem 3.4

Theorem 3.4. *Suppose the target $m(\mathbf{x})$ and the surrogate $\tilde{m}(\mathbf{x})$ are Lipschitz continuous with constants γ_1 and γ_2 , respectively. Assume $m(\mathbf{w}) = \tilde{m}(\mathbf{w})$ for some $\mathbf{w} \in [0, 1]^d$. Then, for any $\mathbf{x} \in [0, 1]^d$, the difference between the outputs of the two models is bounded from above as follows: $|\tilde{m}(\mathbf{x}) - m(\mathbf{x})| \leq (\gamma_1 + \gamma_2)\|\mathbf{x} - \mathbf{w}\|_2$.*

Proof.

$$|\tilde{m}(\mathbf{x}) - m(\mathbf{x})| = |\tilde{m}(\mathbf{x}) - \tilde{m}(\mathbf{w}) - (m(\mathbf{x}) - \tilde{m}(\mathbf{w}))| \quad (16)$$

$$= |\tilde{m}(\mathbf{x}) - \tilde{m}(\mathbf{w}) - (m(\mathbf{x}) - m(\mathbf{w}))| \quad (17)$$

$$\leq \underbrace{|\tilde{m}(\mathbf{x}) - \tilde{m}(\mathbf{w})|}_{\leq \gamma_1 \|\mathbf{x} - \mathbf{w}\|_2} + \underbrace{|m(\mathbf{x}) - m(\mathbf{w})|}_{\leq \gamma_2 \|\mathbf{x} - \mathbf{w}\|_2} \quad (18)$$

$$\leq (\gamma_1 + \gamma_2)\|\mathbf{x} - \mathbf{w}\|_2 \quad (19)$$

where the first inequality is a result of applying the triangle inequality and the second follows from the definition of Lipschitz continuity (Definition 2.7). \square

B Experimental Details and Additional Results

B.1 Details of Real-World Datasets

We use four publicly available real-world tabular datasets (namely, Adult Income, COMPAS, DCCC, and HELOC) to evaluate the performance of the attack proposed in Section 3.2. The details of these datasets are as follows:

- **Adult Income:** The dataset is a 1994 census database with information such as educational level, marital status, age and annual income of individuals (Becker and Kohavi 1996). The target is to predict “income”, which indicates whether the annual income of a given person exceeds \$50000 or not (i.e., $y = \mathbb{1}[\text{income} \geq 0.5]$). It contains 32561 instances in total (the training set), comprising of 24720 from $y = 0$ and 7841 from $y = 1$. To make the dataset class-wise balanced we randomly sample 7841 instances from class $y = 0$, giving a total effective size of 15682 instances. Each instance has 6 numerical features and 8 categorical features. During pre-processing, categorical features are encoded as integers. All the features are then normalized to the range $[0, 1]$.
- **Home Equity Line of Credit (HELOC):** This dataset contains information about customers who have requested a credit line as a percentage of home equity (FICO 2018). It contains 10459 instances with 23 numerical features each. Prediction target is “is_at_risk” which indicates whether a given customer would pay the loan in the future. Dataset is slightly unbalanced with class sizes of 5000 and 5459 for $y = 0$ and $y = 1$, respectively. Instead of using all 23 features, we use the following subset of 10 for our experiments; “estimate_of_risk”, “net_fraction_of_revolving_burden”, “percentage_of_legal_trades”, “months_since_last_inquiry_not_recent”, “months_since_last_trade”, “percentage_trades_with_balance”, “number_of_satisfactory_trades”, “average_duration_of_resolution”, “nr_total_trades”, “nr_banks_with_high_ratio”. All the features are normalized to lie in the range $[0, 1]$.
- **Correctional Offender Management Profiling for Alternative Sanctions (COMPAS):** This dataset has been used for investigating racial biases in a commercial algorithm used for evaluating reoffending risks of criminal defendants (Angwin et al. 2016). It includes 6172 instances and 20 numerical features. The target variable is “is_recid”. Class-wise counts are 3182 and 2990 for $y = 0$ and $y = 1$, respectively. All the features are normalized to the interval $[0, 1]$ during pre-processing.
- **Default of Credit Card Clients (DCCC):** The dataset includes information about credit card clients in Taiwan (Yeh 2016). The target is to predict whether a client will default on the credit or not, indicated by “default.payment.next.month”. The dataset contains 30000 instances with 24 attributes each. Class-wise counts are 23364 from $y = 0$ and 6636 from $y = 1$. To alleviate the imbalance, we randomly select 6636 instances from $y = 0$ class, instead of using all the instances. All the attributes are numerical, and normalized to $[0, 1]$ during pre-processing.

B.2 Experiments on the attack proposed in Section 3.2

In this section, we provide details about our experimental setup with additional results. For convenience, we present the neural network model architectures by specifying the number of neurons in each hidden layer as a tuple, where the leftmost element corresponds to the layer next to the input; e.g.: a model specified as (20,30,10) has the following architecture:

$$\text{Input} \rightarrow \text{Dense}(20, \text{ReLU}) \rightarrow \text{Dense}(30, \text{ReLU}) \rightarrow \text{Dense}(10, \text{ReLU}) \rightarrow \text{Output}(\text{Sigmoid})$$

Other specifications of the models, as detailed below, are similar across most of the experiments. Changes are specified specifically. The hidden layer activations are ReLU and the layer weights are L_2 -regularized. The regularization coefficient is 0.001. Each model is trained for 200 epochs, with a batch size of 32.

Fidelity is evaluated over a uniformly sampled set of input instances (uniform data) as well as a held-out portion of the original data (test data). The experiments were carried out as follows:

1. Initialize the target model. Train using $\mathbb{D}_{\text{train}}$.

2. For $t = 1, 2, \dots, T$:
 - (a) Sample $N \times t$ data points from the dataset to create $\mathbb{D}_{\text{attack}}$.
 - (b) Carry-out the attack given in Algorithm 1 with $\mathbb{D}_{\text{attack}}$. Use $k = 1$ for “Baseline” models and $k = 0.5$ for “Proposed” models.
 - (c) Record the fidelity over \mathbb{D}_{ref} along with t .
3. Repeat steps 1 and 2 for S number of times and calculate average fidelities for each t , across repetitions.

Based on the experiments of Aïvodji, Bolot, and Gambs (2020) and Wang, Qian, and Miao (2022), we select $T, N = 20$ and $S = 100$, unless specified otherwise.

Visualizing the attack using synthetic data This experiment is conducted on a synthetic dataset which consists of 1000 samples generated using the `make_moons` function from the `sklearn` package. Features are normalized to the range $[0, 1]$ before feeding to the classifier. The target model has 4 hidden layers with the architecture (10, 20, 20, 10). The surrogate model is 3-layered with the architecture (10, 20, 20). Each model is trained for 100 epochs. Since the intention of this experiment is to demonstrate the functionality of the modified loss function given in (4), a large query of size 200 is used, instead of performing multiple small queries. Fig. 6 shows how the original model extraction attack proposed by (Aïvodji, Bolot, and Gambs 2020) suffers from the boundary shift issue, while the model with the proposed loss function overcomes this problem. Fig. 10 illustrates the instances misclassified by the two surrogate models.

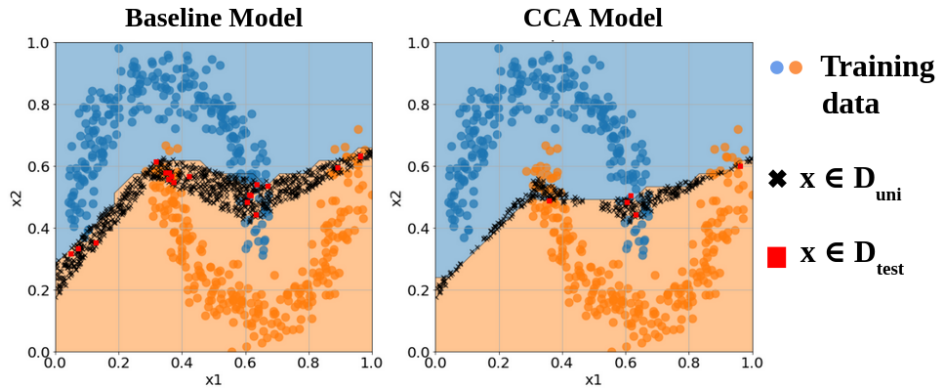


Figure 10: Misclassifications w.r.t. to the target model, over \mathbb{D}_{uni} and \mathbb{D}_{test} as the reference datasets for the 2-dimensional demonstration in Fig. 6. “Baseline” model causes a large number of misclassifications w.r.t. the “CCA” model.

Comparing performance over four real-world dataset We use a target model having 2 hidden layers with the architecture (20,10). Two surrogate model architectures, one exactly similar to the target architecture (model 0 - known architecture) and the other slightly different (model 1 - unknown architecture), are tested. Model 1 has 3 hidden layers with the architecture (20,10,5).

Fig. 11 illustrates the fidelities achieved by the two model architectures described above. Fig. 12 shows the corresponding variances of the fidelity values over 100 realizations. It can be observed that the variances diminish as the query size grows, indicating more stable model extractions. Fig. 13 demonstrates the effect of the proposed loss function in mitigating the decision boundary shift issue.

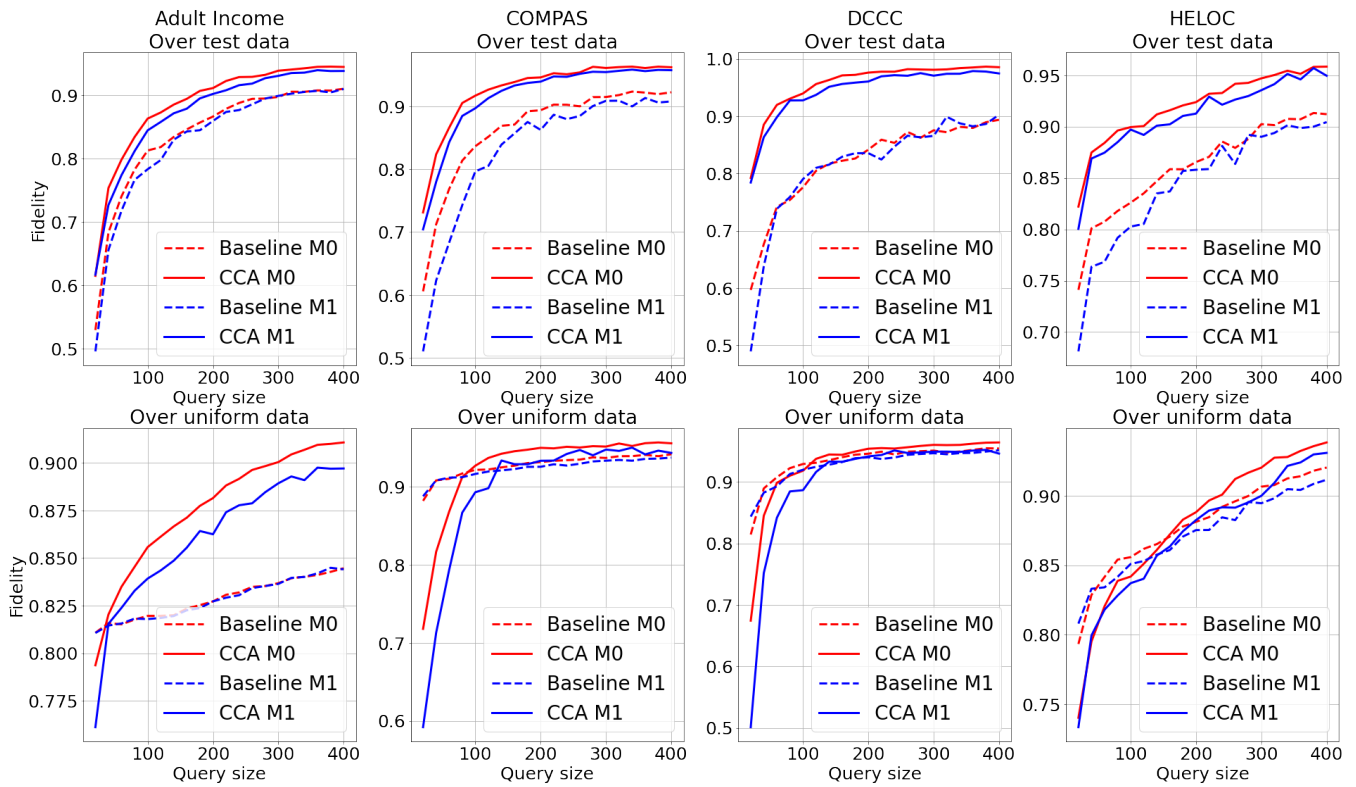


Figure 11: Fidelity for real-world datasets. Solid lines indicate “CCA” models. Dashed lines indicate “Baseline” models. Colors correspond to the model architecture, i.e., red: model 0, blue: model 1.

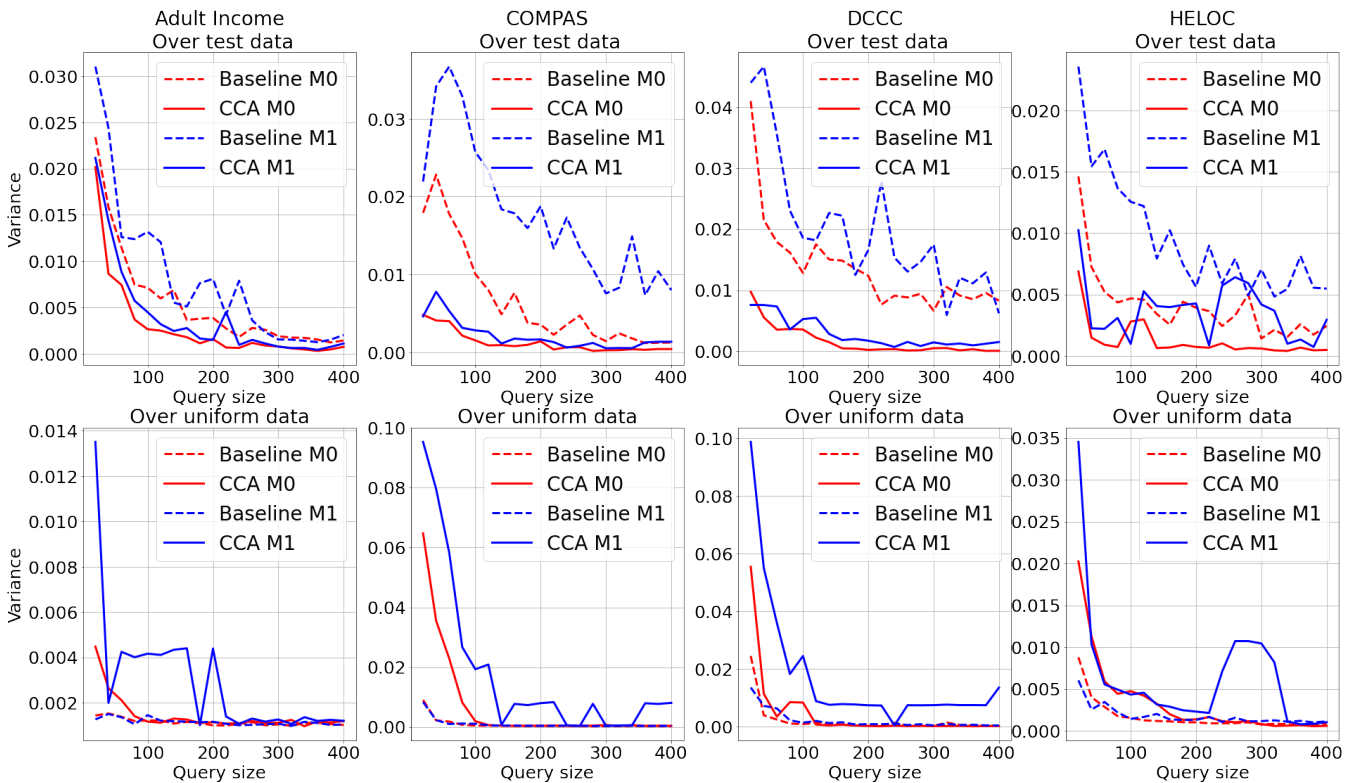


Figure 12: Variance of fidelity for real-world datasets. Solid lines indicate “CCA” models. Dashed lines indicate “Baseline” models. Colors correspond to the model architecture, i.e., red: model 0, blue: model 1.

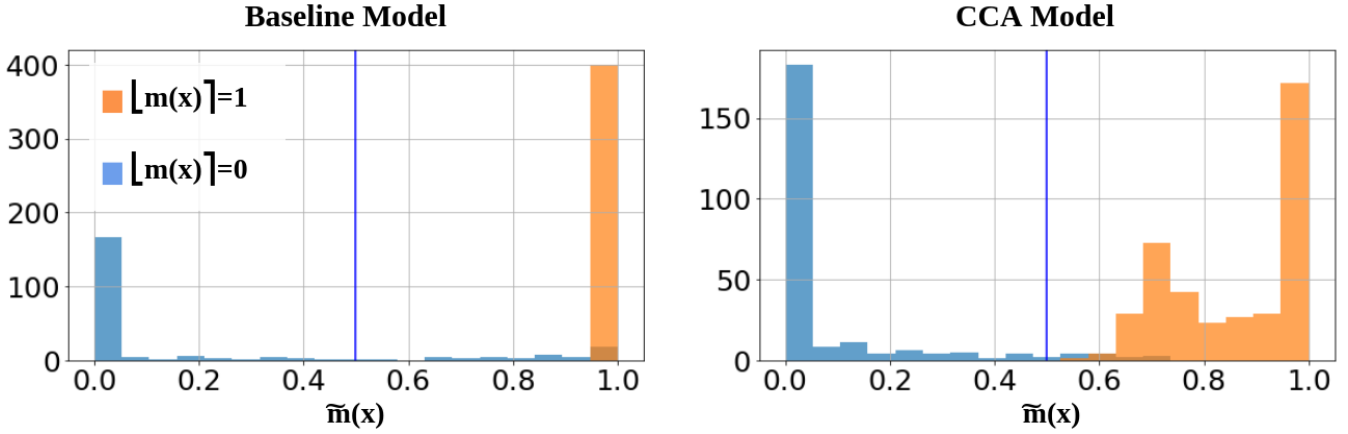


Figure 13: Histograms of probabilities predicted by “Baseline” and “CCA” models under the “Unknown Architecture” scenario (model 1) for the HELOC dataset. Note how the “Baseline” model provides predictions higher than 0.5 for a comparatively larger number of instances with $[m(\boldsymbol{x})] = 0$ due to the boundary shift issue. The clamping effect of the novel loss function is evident in the “CCA” model’s histogram, where the decision boundary being held closer to the counterfactuals is causing the two prominent modes in the favorable region. The mode closer to 0.5 is due to counterfactuals and the mode closer to 1.0 is due to instances with $[m(\boldsymbol{x})] = 1$.

Empirical and theoretical rates of convergence Fig. 14 compares the rate of convergence of the empirical approximation error i.e., $1 - \mathbb{E} [\text{Fid}_{m, \mathbb{D}_{\text{ref}}}(\tilde{M}_n)]$ for two of the above experiments with the rate predicted by Theorem A.3. Notice how the empirical error decays faster than $n^{-2/(d-1)}$.

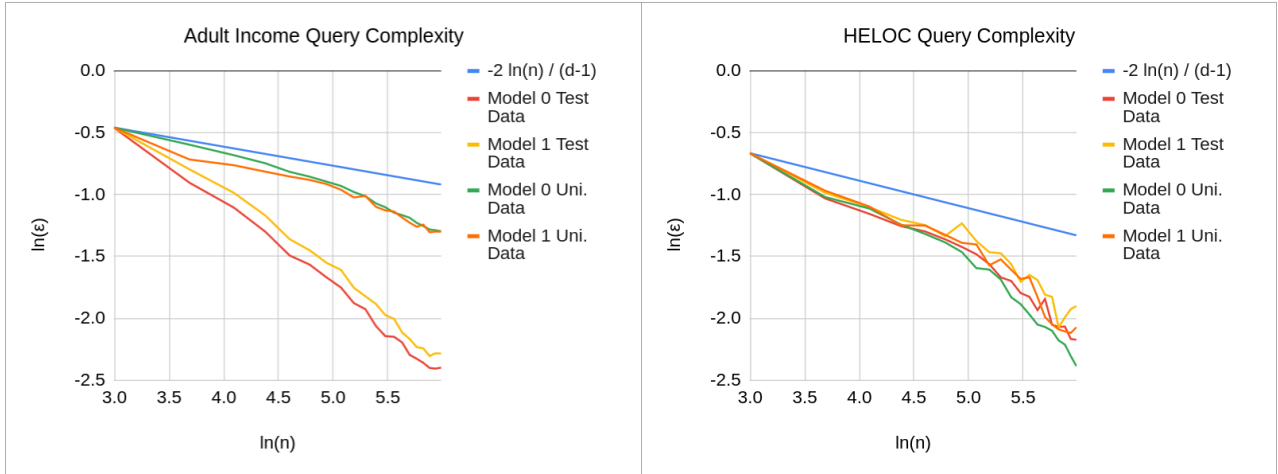


Figure 14: A comparison of the query complexity derived in Theorem 3.2 with the empirical query complexities obtained on the Adult Income and HELOC datasets. The graphs are on a log-log scale. We observe that the analytical query complexity is an upper bound for the empirical query complexities. All the graphs are recentered with an additive constant for presentational convenience. However, this does not affect the slope of the graph, which corresponds to the complexity.

Studying effects of Lipschitz constants For this experiment, we use a target model having 3 hidden layers with the architecture (20, 10, 5) and a surrogate model having 2 hidden layers with the architecture (20, 10). The surrogate model layers are L_2 -regularized with a fixed regularization coefficient of 0.001. We achieve different Lipschitz constants for the target models by controlling their L_2 -regularization coefficients during the target model training step. Following (Gouk et al. 2021), we approximate the Lipschitz constant of target models by the product of the spectral norms of the weight matrices.

Fig. 7 illustrates the dependence of the attack performance on the Lipschitz constant of the target model. The results lead to the conclusion that target models with larger Lipschitz constants are more difficult to extract. This follows the insight provided by Theorem 3.4.

Studying different model architectures We use the HELOC dataset for this experiment. The target model has a fixed architecture of (20, 30, 10). Surrogate model architectures are given in Table 2, ranging from very complex to much simpler than the target model. The ensemble size S is selected to be 50.

Table 2: Surrogate model architectures

Model	Hidden layers
Model 0	(30, 20, 20, 10)
Model 1	(20, 30, 10)
Model 2	(20, 10)
Model 3	(5, 5)

Results (see Fig. 15) indicate that the performance is weakly dependent on the model architecture as long as the surrogate models are closer to the target model in complexity, which is an observation made also by Aivodji, Bolot, and Gambis (2020). Results of additional experiments with varying target and surrogate model architectures are presented in Table 3 and 4.

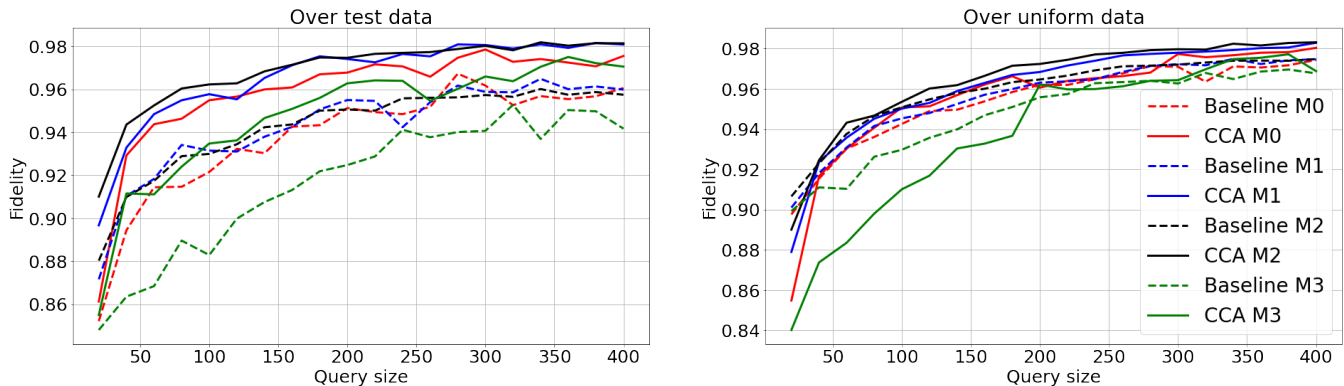


Figure 15: Effect of the surrogate model architecture on the attack performance. Dashed lines correspond to “Baseline” models and solid lines represent the “CCA” models. See Table 2 for the model specifications. The attack performance is weakly dependent on the surrogate model architecture as long as it is closer to the complexity of the target model.

Studying alternate counterfactual generating method Counterfactuals can be generated such that they satisfy additional desirable properties such as actionability, sparsity and closeness to the data manifold, other than the proximity to the original instance. In this experiment, we observe how counterfactuals with above properties affect the attack performance. DCCC is used as the dataset. Target model has the architecture (20, 30, 10) and the architecture of the surrogate model is (10, 20).

To generate actionable counterfactuals, we use Diverse Counterfactual Explanations (DiCE) by Mothilal, Sharma, and Tan (2020) with features “SEX”, “MARRIAGE”, and “AGE” kept unchanged. The diversity factor of DiCE generator is set to 1 in order to obtain only a single counterfactual for each query. Sparse counterfactuals are obtained by the same MCCC generator used in other experiments, but now with L_1 norm as the cost function $c(\mathbf{x}, \mathbf{w})$. Counterfactuals from the data manifold (i.e., realistic counterfactuals, denoted by 1-NN) are generated using a 1-Nearest-Neighbour algorithm. Table 5 summarizes the performance of the attack.

When the counterfactuals lie further away from the decision boundary, the advantage of the proposed attack w.r.t. the baseline diminishes. In order to observe this effect, we carry-out the attacks using counterfactuals with two different levels of sparsity. It can be observed that when the sparsity increases, the counterfactuals tend to lie further away from the decision boundary (see Fig. 16). Accordingly, the performance gap between the CCA and the baseline attacks diminishes, as seen in Fig. 17.

Studying effect of unbalanced $\mathbb{D}_{\text{attack}}$ In all the other experiments, the attack dataset $\mathbb{D}_{\text{attack}}$ used by the adversary is sampled from a class-wise balanced dataset. In this experiment we explore the effect of querying using an unbalanced $\mathbb{D}_{\text{attack}}$. Model architectures used are (20, 10) for the target model and surrogate model 0, and (20, 10, 5) for surrogate model 1.

Two versions of the Adult Income dataset were used in the experiment. The first version, used in Fig. 18a contains 24720 and 7841 examples from classes $y = 0$ and $y = 1$, respectively. The second version corresponding to Fig. 18b contains 2472 and 7841 examples from classes $y = 0$ and $y = 1$, respectively. The proposed attack surpasses the baseline attack in both scenarios.

Studying other machine learning models We explore the effectiveness of the proposed attack when the target model is no longer a neural network classifier. The surrogate models are still neural networks with the architectures (20, 10) for model 0

Table 3: Fidelity over \mathbb{D}_{test} and \mathbb{D}_{uni} for datasets DCCC and HELOC

Dataset: DCCC - Fidelity over \mathbb{D}_{test}												
Target archi. \rightarrow	(20,10)				(20,10,5)				(20,20,10,5)			
	100 queries		200 queries		100 queries		200 queries		100 queries		200 queries	
Surrogate archi. \downarrow	Base.	CCA	Base.	CCA	Base.	CCA	Base.	CCA	Base.	CCA	Base.	CCA
(20,10)	0.96	0.98	0.97	0.99	0.96	0.99	0.97	0.99	0.91	0.97	0.92	0.98
(20,10,5)	0.96	0.98	0.97	0.99	0.94	0.97	0.96	0.98	0.91	0.97	0.92	0.97
(20,20,10,5)	0.93	0.97	0.94	0.98	0.92	0.97	0.93	0.97	0.88	0.94	0.92	0.96
Dataset: DCCC - Fidelity over \mathbb{D}_{uni}												
Target archi. \rightarrow	(20,10)				(20,10,5)				(20,20,10,5)			
	100 queries		200 queries		100 queries		200 queries		100 queries		200 queries	
Surrogate archi. \downarrow	Base.	CCA	Base.	CCA	Base.	CCA	Base.	CCA	Base.	CCA	Base.	CCA
(20,10)	0.95	0.96	0.96	0.97	0.97	0.97	0.97	0.98	0.98	0.98	0.98	0.98
(20,10,5)	0.94	0.96	0.95	0.96	0.95	0.94	0.94	0.96	0.97	0.98	0.98	0.98
(20,20,10,5)	0.92	0.93	0.95	0.94	0.96	0.94	0.95	0.96	0.94	0.92	0.96	0.94
Dataset: HELOC - Fidelity over \mathbb{D}_{test}												
Target archi. \rightarrow	(20,10)				(20,10,5)				(20,20,10,5)			
	100 queries		200 queries		100 queries		200 queries		100 queries		200 queries	
Surrogate archi. \downarrow	Base.	CCA	Base.	CCA	Base.	CCA	Base.	CCA	Base.	CCA	Base.	CCA
(20,10)	0.90	0.94	0.91	0.95	0.90	0.94	0.92	0.95	0.98	0.99	0.98	0.99
(20,10,5)	0.88	0.92	0.92	0.95	0.89	0.92	0.92	0.95	0.98	0.98	0.98	0.99
(20,20,10,5)	0.87	0.93	0.91	0.93	0.87	0.89	0.91	0.94	0.98	0.98	0.98	0.98
Dataset: HELOC - Fidelity over \mathbb{D}_{uni}												
Target archi. \rightarrow	(20,10)				(20,10,5)				(20,20,10,5)			
	100 queries		200 queries		100 queries		200 queries		100 queries		200 queries	
Surrogate archi. \downarrow	Base.	CCA	Base.	CCA	Base.	CCA	Base.	CCA	Base.	CCA	Base.	CCA
(20,10)	0.92	0.92	0.94	0.95	0.91	0.91	0.94	0.95	0.98	0.98	0.99	0.99
(20,10,5)	0.91	0.90	0.94	0.93	0.91	0.89	0.93	0.94	0.97	0.97	0.98	0.99
(20,20,10,5)	0.91	0.91	0.93	0.94	0.91	0.87	0.93	0.92	0.97	0.97	0.98	0.98

and (20, 10, 5) for model 1. A random forest classifier with 100 estimators and a linear regression classifier, trained on Adult Income dataset are used as the targets. Ensemble size S used is 20. Results are shown in Fig. 19, where the proposed attack performs better or similar to the baseline attack.

Studying alternate loss functions We explore using binary cross-entropy loss function directly with labels 0, 1 and 0.5 in place of the proposed loss. Precisely, the surrogate loss is now defined as

$$L(\tilde{m}, y) = -y(\mathbf{x}) \log(\tilde{m}(\mathbf{x})) - (1 - y(\mathbf{x})) \log(1 - \tilde{m}(\mathbf{x})) \quad (20)$$

which is symmetric around 0.5 for $y(\mathbf{x}) = 0.5$. Two surrogate models are observed, with architectures (20, 10) for model 0 and (20, 10, 5) for model 1. The target model’s architecture is similar to that of model 0. The ensemble size is $S = 20$.

The results (in Fig. 20) indicate that the binary cross-entropy loss performs worse than the proposed loss. The reason might be the following: As the binary cross-entropy loss is symmetric around 0.5 for counterfactuals, it penalizes the counterfactuals that are farther inside the favorable region. This in turn pulls the surrogate decision boundary towards the favorable region more than necessary, causing a decision boundary shift.

B.3 Experiments for verifying Theorem 3.2

This experiment includes approximating a spherical decision boundary in the first quadrant of a d -dimensional space. The decision boundary is a portion of a sphere with radius 1 and the origin at $(1, 1, \dots, 1)$. The input space is assumed to be normalized, and hence, restricted to the unit hypercube. See Section 3.1 for a description of the attack strategy. Fig. 21 presents a visualization of the experiment in the case where the dimensionality $d = 2$. Fig. 8 presents a comparison of theoretical and empirical query complexities for higher dimensions. Experiments agree with the theoretical upper-bound.

Table 4: Fidelity over \mathbb{D}_{test} and \mathbb{D}_{uni} for datasets Adult Income and COMPAS

Dataset: Adult Income - Fidelity over \mathbb{D}_{test}												
Target archi. →	(20,10)				(20,10,5)				(20,20,10,5)			
	100 queries		200 queries		100 queries		200 queries		100 queries		200 queries	
Surrogate archi. ↓	Base.	CCA	Base.	CCA	Base.	CCA	Base.	CCA	Base.	CCA	Base.	CCA
(20,10)	0.88	0.89	0.92	0.93	0.82	0.84	0.91	0.93	0.94	0.95	0.95	0.96
(20,10,5)	0.87	0.88	0.91	0.93	0.79	0.82	0.90	0.92	0.93	0.94	0.95	0.96
(20,20,10,5)	0.85	0.86	0.91	0.91	0.79	0.81	0.89	0.92	0.93	0.92	0.95	0.95
Dataset: Adult Income - Fidelity over \mathbb{D}_{uni}												
Target archi. →	(20,10)				(20,10,5)				(20,20,10,5)			
	100 queries		200 queries		100 queries		200 queries		100 queries		200 queries	
Surrogate archi. ↓	Base.	CCA	Base.	CCA	Base.	CCA	Base.	CCA	Base.	CCA	Base.	CCA
(20,10)	0.71	0.81	0.75	0.87	0.78	0.84	0.79	0.87	0.84	0.88	0.85	0.91
(20,10,5)	0.71	0.78	0.74	0.83	0.77	0.82	0.78	0.85	0.82	0.88	0.84	0.90
(20,20,10,5)	0.71	0.75	0.74	0.81	0.77	0.81	0.78	0.84	0.82	0.86	0.84	0.90
Dataset: COMPAS - Fidelity over \mathbb{D}_{test}												
Target archi. →	(20,10)				(20,10,5)				(20,20,10,5)			
	100 queries		200 queries		100 queries		200 queries		100 queries		200 queries	
Surrogate archi. ↓	Base.	CCA	Base.	CCA	Base.	CCA	Base.	CCA	Base.	CCA	Base.	CCA
(20,10)	0.93	0.96	0.94	0.97	0.92	0.94	0.94	0.96	0.94	0.96	0.95	0.97
(20,10,5)	0.92	0.95	0.94	0.97	0.92	0.93	0.95	0.95	0.94	0.96	0.95	0.97
(20,20,10,5)	0.92	0.95	0.92	0.97	0.84	0.91	0.89	0.94	0.92	0.94	0.94	0.96
Dataset: COMPAS - Fidelity over \mathbb{D}_{uni}												
Target archi. →	(20,10)				(20,10,5)				(20,20,10,5)			
	100 queries		200 queries		100 queries		200 queries		100 queries		200 queries	
Surrogate archi. ↓	Base.	CCA	Base.	CCA	Base.	CCA	Base.	CCA	Base.	CCA	Base.	CCA
(20,10)	0.94	0.95	0.94	0.96	0.95	0.95	0.95	0.96	0.96	0.95	0.96	0.96
(20,10,5)	0.93	0.95	0.94	0.95	0.94	0.92	0.95	0.92	0.95	0.96	0.96	0.96
(20,20,10,5)	0.93	0.94	0.94	0.95	0.94	0.85	0.94	0.90	0.95	0.92	0.95	0.94

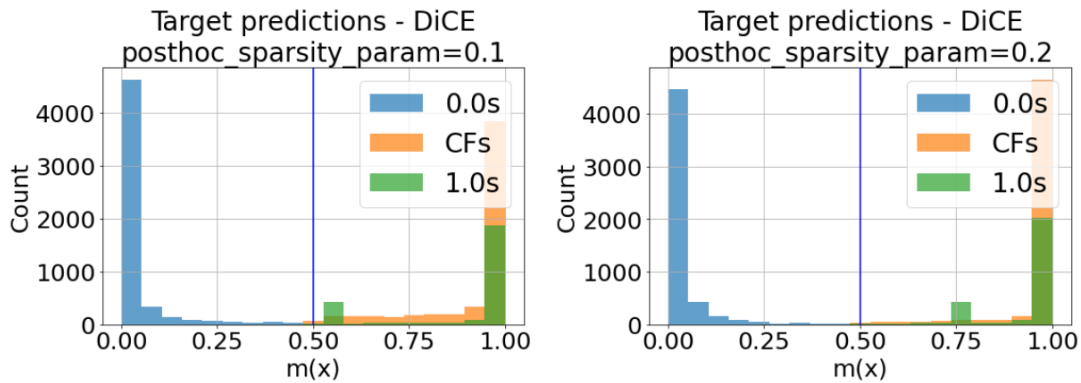


Figure 16: Histogram of target model predictions $m(\mathbf{x})$ for instances with $\lfloor m(\mathbf{x}) \rfloor = 0, 1$ and counterfactuals, when different levels of sparsity is used with DiCE. Higher the parameter 'posthoc_sparsity_param', more sparse the counterfactuals are. Note how the predictions on counterfactuals are concentrated away from the decision boundary when the sparsity is high. Dataset used is DCCC.

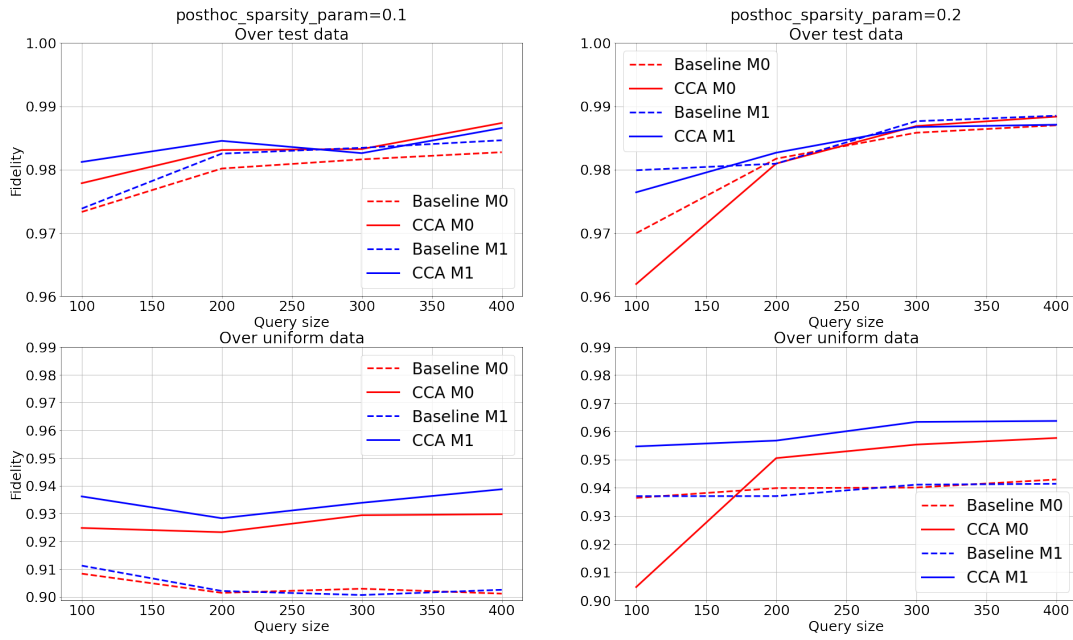
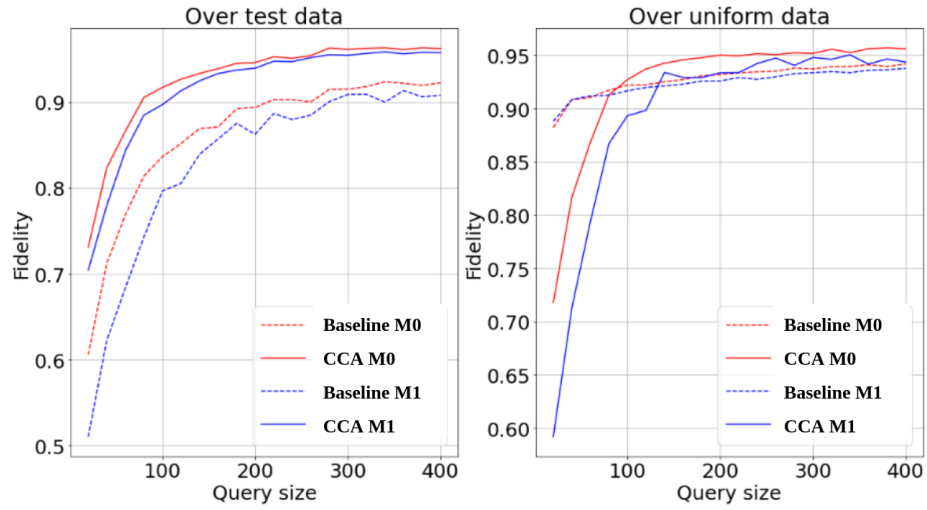


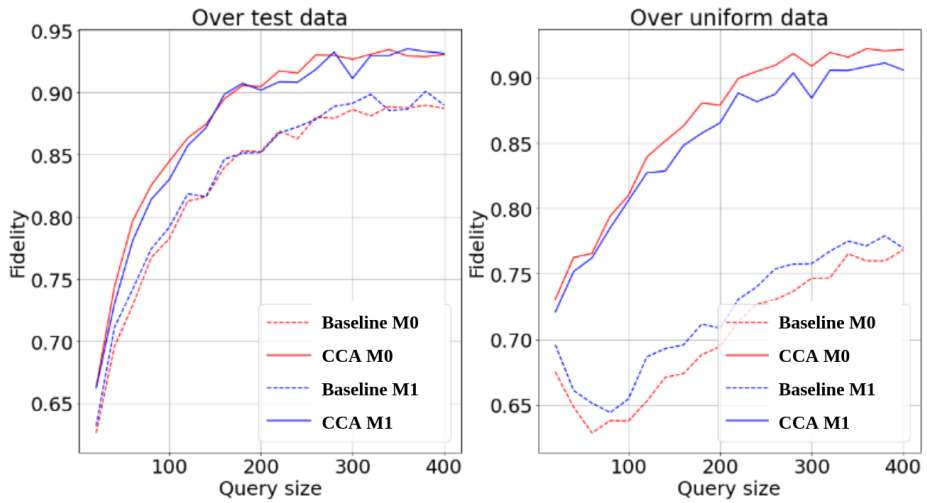
Figure 17: Attack performance on DCCC dataset when different levels of sparsity in DiCE is used. Higher the parameter 'posthoc_sparsity_param', more sparse the counterfactuals are.

Table 5: Fidelity achieved with different counterfactual generating methods on DCCC dataset. Target model has hidden layers with neurons (20, 30, 10). Surrogate model architecture is (10, 20).

CF method	Fidelity over \mathbb{D}_{test}				Fidelity over \mathbb{D}_{uni}			
	100 queries		200 queries		100 queries		200 queries	
	Base.	CCA	Base.	CCA	Base.	CCA	Base.	CCA
MCCF L2-norm	0.98	0.99	0.98	0.99	0.95	0.96	0.95	0.97
MCCF L1-norm	0.79	0.95	0.85	0.97	0.89	0.92	0.93	0.94
DiCE Actionable	0.98	0.98	0.98	0.98	0.92	0.94	0.91	0.94
1-NN	0.98	0.99	0.99	0.99	0.94	0.95	0.95	0.96



(a)



(b)

Figure 18: Results corresponding to the Adult Income dataset with queries sampled from biased versions of the dataset (i.e., a biased $\mathbb{D}_{\text{attack}}$). The version used in Fig. 18a contains 24720 and 7841 examples from classes $y = 0$ and $y = 1$, respectively. The version corresponding to Fig. 18b contains 2472 and 7841 examples from classes $y = 0$ and $y = 1$, respectively.

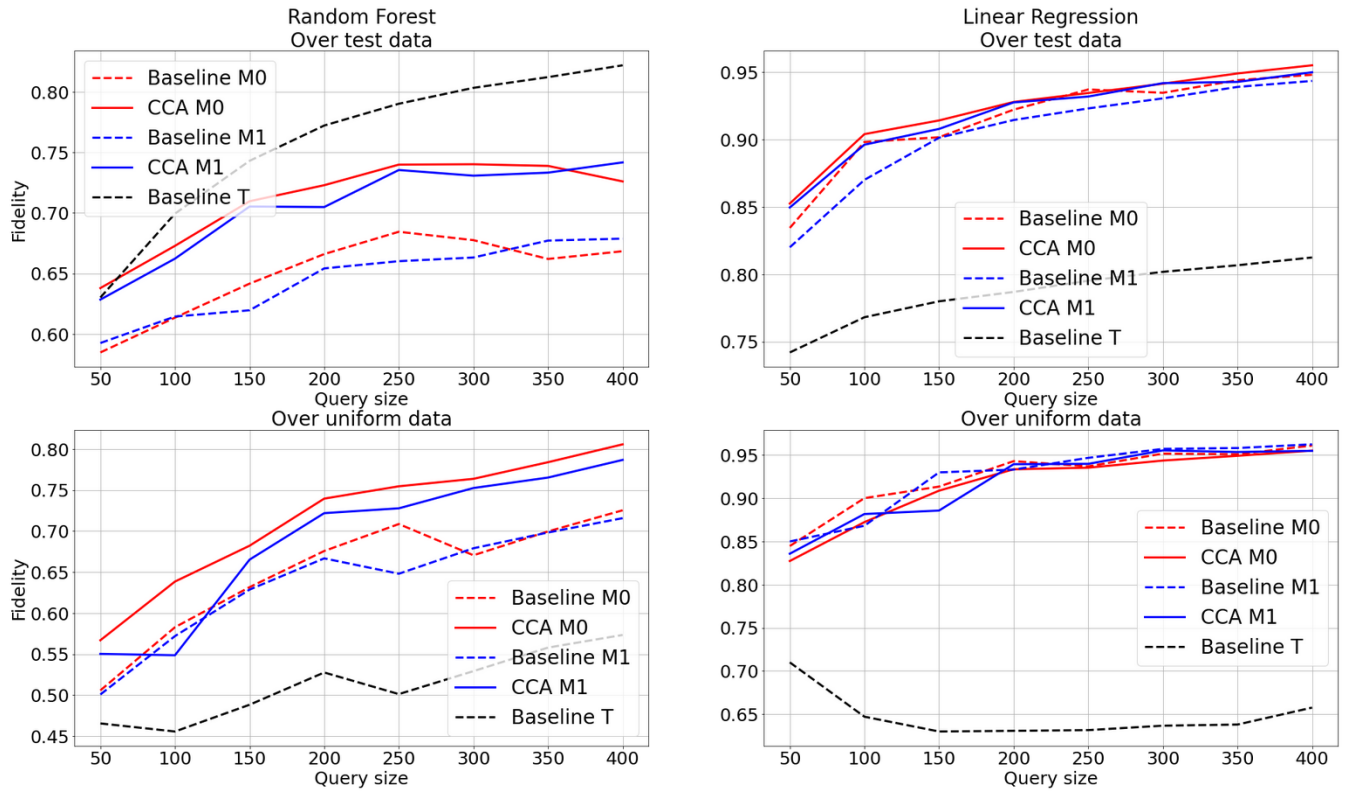


Figure 19: Performance of the attack when the target model is not a neural network. Surrogates M0 and M1 are neural networks with the architectures (20,10) and (20,10,5) respectively. Baseline T is a surrogate model from the same class as the target model.

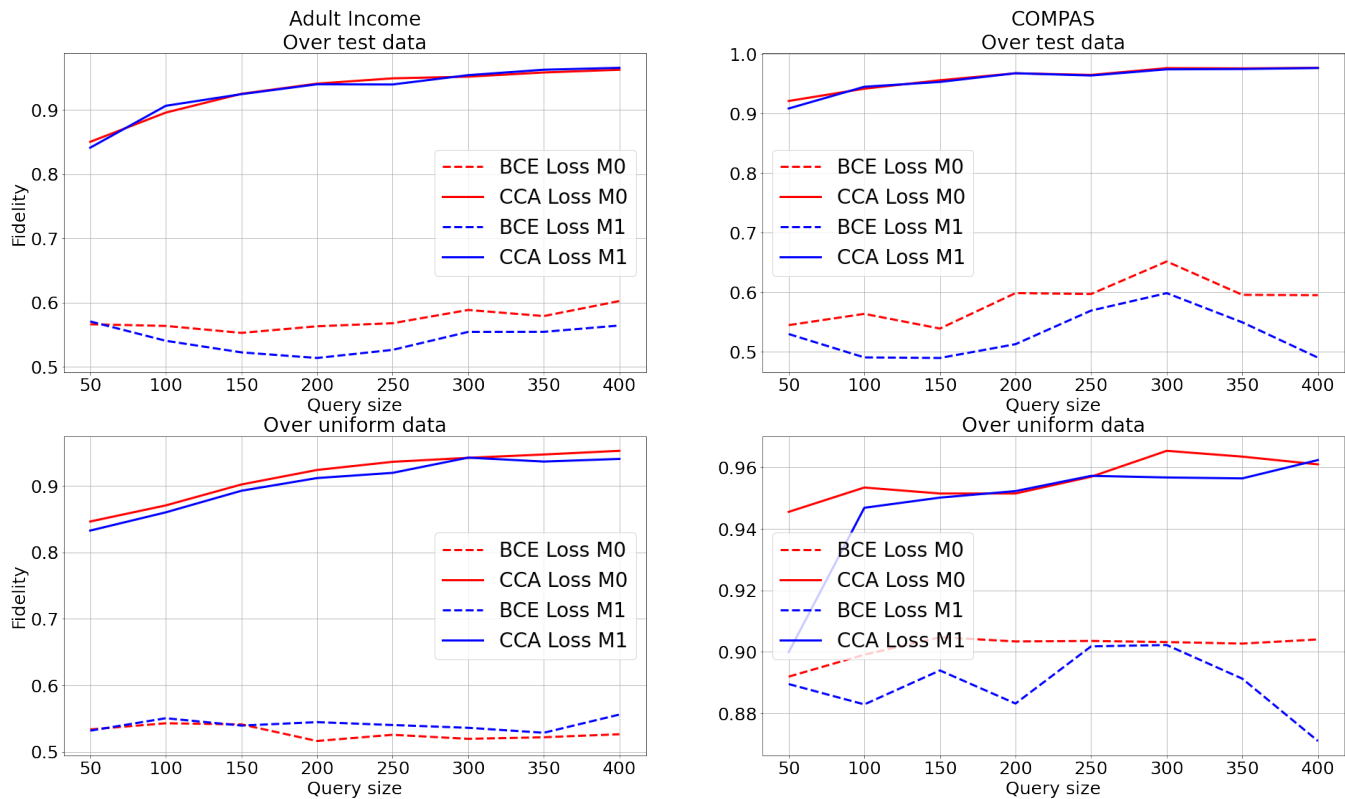


Figure 20: Performance of binary cross-entropy loss with labels 0, 0.5 and 1. Dashed lines corresponding to binary cross entropy (BCE) loss and solid lines depict the performance of the CCA loss.

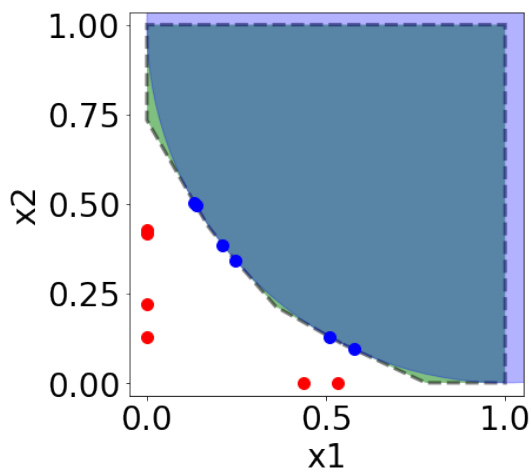


Figure 21: Synthetic attack for verifying Theorem 3.2 in the 2-dimensional case. Red dots represent queries and blue dots are the corresponding closest counterfactuals. Dashed lines indicate the boundary of the polytope approximation.